Electronic Supporting Information

Phenoxybis(imine) complexes of vanadium: structure, ethylene polymerization and ring opening polymerization of ε-caprolactone

Yi Gong,[a] Kaname Shibata,[b] Kenji Michiue,[b] Joseph Gbertyo,[a,c] Zaid Rais,[a] Mark R. J. Elsegood,[d] Timothy J. Prior[e] and Carl Redshaw[f*]

[a] *Plastics Collaboratory, Chemistry, School of Natural Sciences, University of Hull, Cottingham Road, Hull, HU6 7RX, U.K.*

[b] *R&D Centre, Mitsui Chemical Inc., 580-32 Naguara, Sodegaura, Chiba 299-0265, Japan*

[c] *Department of Chemistry, Faculty of Science, Benue State University, Makurdi, Nigeria.*

[d] *Chemistry Department, Loughborough University, Loughborough, Leicestershire, LE11 3TU, U.K.*

[e] *Department of Chemistry, University of Liverpool, Crown Street, Liverpool, L69 7ZD, UK*

[f] *Department of Chemistry, Graduate School of Science, Tokyo Metropolitan University, 1-1 Minami Osawa, Hachioji, Tokyo, 192-0397, Japan*

Contents list

Experimental for the pro-ligands (*p*-RL^{n}H) (n = 1 – 7, R = Me, *t*-Bu)

Synthesis of p-MeL^{1}H

To 2,6-dimethylaniline (1.48 g, 12.2 mmol) and 2,6-diformyl-4-methylphenol (1.00 g, 6.09 mmol) in ethanol (40 mL) was added a few drops of formic acid. The system was refluxed for 6 h and then, on cooling, the volatiles were removed under vacuo to about half volume. A yellow precipitate was isolated, washed with cold methanol (30 mL) and dried *in vacuo*. Crystallization from a saturated acetonitrile solution at ambient temperature afforded pale-yellow crystals. Yield: 1.83 g, 81%. IR: 2375w, 2290w, 2222w, 1673s, 1626s, 1587s, 1306s, 1261s, 1225m, 1190s, 1158s, 1123s, 1088s, 1028s, 982m, 971s, 912w, 861m, 801s, 770s, 756m, 723s, 685w. This compound has previously been reported in reference [S1].

Synthesis of p-t-BuL^{1}H

As for *p*-MeL^{1}H, but using 2,6-dimethylaniline (1.18 g, 1.20 mL, 9.74 mmol) and 2,6-diformyl-4-*t*-butylphenol (1.00 g, 4.85 mmol) affording *p-t*-BuL^{1}H as a yellow solid. Crystallization from a saturated acetonitrile solution at ambient temperature afforded pale-yellow needles. Yield: 1.54 g, 77%. IR: 1628s, 1589s, 1317m, 1281m, 1265m, 1228m, 1196m, 1186s, 1120w, 1089m, 1033m, 1005s, 984m, 917w, 890w, 868w, 857m, 821m, 796m, 763s, 748m, 724m, 696w, 637w. Other data has been reported in reference [S2].

Synthesis of p-MeL^{2}H

As for *p*-MeL^{1}H, but using 2,6-diisopropylaniline (2.16 g, 12.2 mmol) and 2,6-diformyl-4-methylphenol (1.00 g, 6.09 mmol) affording *p*-MeL^{2}H as a yellow solid. Yield: 2.29 g, 78%. IR: 1631s, 1587m, 1459m, 1383s, 1354m, 1310m, 1280s, 1257m,

1224s, 1181s, 1157s, 1099w, 1035m, 978s, 932s, 854m, 789s, 758m, 698s, 632s, 597s, 550m. This compound has previously been reported in reference [S1].

*Synthesis of p-t-*BuL^{2}H

As for *p*-MeL^{1}H, but using 2,6-diisopropylaniline (1.72 g, 9.70 mmol) and 2,6-diformyl-4-*t*-butylphenol (1.00 g, 4.85 mmol) affording *p-t-*BuL^{2}H as a yellow solid. Yield: 2.09 g, 82%. IR: 1629s, 1585m, 1308s, 1283s, 1263s, 1223m, 1175s, 1098m, 1058m, 102m, 1006s, 963m, 933m, 888m, 869w, 856m, 820m, 798m, 786w, 766m, 755m, 723s, 632w. Other data has been reported in reference [S2].

*Synthesis of p-*MeL^{3}H

As for *p*-MeL^{1}H, but using 2-*t*-butylaniline (1.82 g, 12.2 mmol) and 2,6-diformyl-4-methylphenol (1.00 g, 6.09 mmol) affording *p*-MeL^{3}H as an orange solid. Crystallization from a saturated acetonitrile solution at ambient temperature afforded large orange needle-shaped crystals. Yield: 1.87 g, 72%. Found C 81.19, H 8.23, N 6.71%. $C_{29}H_{34}N_2O$ (sample dried *in vacuo* for 2 h) requires C 81.65, H 8.03, N 6.57%. IR: 1627m, 1584m, 1567m, 1352m, 1316m, 1288w, 1257m, 1227m, 1202m, 1158w, 1087w, 1054w, 1038w, 990w, 977m, 941w, 868w, 829w, 757s, 742m, 722m. Mass Spec (*m/z*): 427 (MH^+). ^{1}H NMR (DMSO-d_6) δ: 1.40 (18H, s), 2.37 (3H, s), 7.01 (2H, d, *J* = 7.4 Hz), 7.22 (2H, t, *J* = 7.2 Hz), 7.29 (2H, t, *J* = 7.1 Hz), 7.39 (2H, d, *J* = 7.6 Hz), 7.83 (2H, s), 8.74 (2H, s). The absence of the hydroxyl proton (-OH) signal in the NMR spectrum is likely due to rapid proton exchange with the solvent.

*Synthesis of p-t-*BuL^{3}H

As for *p*-MeL^{1}H, but using 2-*t*-butylaniline (1.45 g, 9.72 mmol) and 2,6-diformyl-4-*t*-butylphenol (1.00 g, 4.85 mmol) affording *p-t-*BuL^{3}H as an orange solid. Crystallization from a saturated acetonitrile solution at ambient temperature afforded orange crystals. Yield: 1.68 g, 74%. Found C 81.02, H 8.65, N 6.29%. $C_{32}H_{40}N_2O$ (sample dried *in vacuo* for 2 h) requires C 81.65, H 8.03, N 6.57%. IR: 1625s, 1582s, 1567m, 1283s, 1261m, 1233m, 1189m, 1163m, 1085m, 1052m, 1031m, 1012s, 968m,

938m, 887m, 876m, 868m, 959m, 820m, 785m, 749s, 723s, 646w, 636w, 617w. Mass Spec (*m/z*): 469 (M^+). ^{1}H NMR (DMSO-d_6) δ: 1.36 (9H, s), 1.42 (18H, s), 6.67 (1H, br), 7.07 (2H, dd, *J* = 7.7, 1.5 Hz), 7.23 (2H, td, *J* = 7.6, 1.5 Hz), 7.30 (2H, td, *J* = 7.5, 1.5 Hz), 7.40 (2H, dd, *J* = 7.8, 1.5 Hz), 8.13 (2H, s), 8.80 (2H, s).

Synthesis of p-MeL^{4}H

As for *p*-MeL^{1}H, but using 2-iodoaniline (2.67 g, 12.2 mmol) and 2,6-diformyl-4-methylphenol (1.00 g, 6.09 mmol) affording *p*-MeL^{4}H as an orange solid. Crystallization from a saturated acetonitrile solution at ambient temperature afforded large orange/red prisms. Yield: 2.34 g, 68%. Found C 44.74, H 2.72, N 4.78%. $C_{21}H_{16}N_2I_2O$ (sample dried *in vacuo* for 2 h) requires C 44.55, H 2.85, N 4.95%. IR: 1619s, 1593s, 1567s, 1318s, 1263s, 1202s, 1160m, 1036w, 1014s, 980m, 858w, 807w, 792w, 763w, 745s, 671m, 635w. Mass Spec (*m/z*): 568 (MH_2^{2+}). ^{1}H NMR (DMSO-d_6) δ: 2.38 (3H, s), 7.06 (2H, td, *J* = 7.7, 1.5 Hz), 7.37 (2H, dd, *J* = 7.9, 1.3 Hz), 7.49 (2H, td, *J* = 7.8, 1.3 Hz), 7.88 (2H, s), 7.96 (2H, dd, *J* = 7.8, 1.2 Hz), 8.86 (2H, s). The absence of the hydroxyl proton (-OH) signal in the NMR spectrum is likely due to rapid proton exchange with the solvent.

Synthesis of p-t-BuL^{4}H

As for *p*-MeL^{1}H, but using 2-iodoaniline (2.13 g, 9.72 mmol) and 2,6-diformyl-4-*t*-butylphenol (1.00 g, 4.85 mmol) affording *p-t*-BuL^{4}H as a yellow solid. Crystallization from a saturated acetonitrile solution at ambient temperature afforded golden needle-shaped crystals. Yield: 2.12 g, 72%. Found C 47.28, H 3.51, N 4.50%. $C_{24}H_{22}N_2I_2O$ (sample dried *in vacuo* for 2 h) requires C 47.39, H 3.65, N 4.61%. IR: 1624m, 1593m, 1571m, 1312m, 1288m, 1264m, 1244m, 1214m, 1199m, 1168m, 1159m, 1124w, 1035m, 1014s, 976s, 934m, 887m, 862w, 850w, 824w, 774m, 763m, 749s, 721s, 665m, 635w, 618w. Mass Spec (*m/z*): 609 (MH^+). ^{1}H NMR (DMSO-d_6) δ: 1.37 (9H, s), 7.04-7.09 (2H, m), 7.40 (2H, dd, *J* = 8.0, 1.4 Hz), 7.47-7.54 (2H, m), 7.96 (2H, dd, *J* = 7.9, 1.3 Hz), 8.18 (2H, s), 8.93 (2H, s). The absence of the hydroxyl proton (-OH) signal in the NMR spectrum is likely due to rapid proton exchange with the solvent.

Synthesis of p-MeL^{5}H

As for *p*-MeL^{1}H, but using pentafluoroaniline (2.23 g, 12.2 mmol) and 2,6-diformyl-4-methylphenol (1.00 g, 6.09 mmol) affording *p*-MeL^{5}H as a yellow solid. Crystallization from a saturated acetonitrile solution at ambient temperature afforded large yellow needle-shaped crystals. Yield: 2.47 g, 82%. Found C 51.06, H 1.40, N 5.50%. $C_{21}H_8N_2F_{10}O$ (sample dried *in vacuo* for 2 h) requires C 51.05, H 1.63, N 5.67%. IR: 3405w, 3175w, 1747w, 1695w, 1682w, 1655m, 1622m, 1607m, 1583m, 1530m, 1505s, 1316s, 1278m, 1228m, 1164m, 1075w, 1046w, 1010s, 996s, 981s, 960s, 891w, 875w, 840m, 820w, 799w, 761m, 722s, 668w, 642w. Mass Spec (*m/z*): 495 (MH^+).^{1}H NMR (DMSO-d_6) δ: 1.32 (3H, d, J = 4.6 Hz), 7.97 (2H, s), 9.14 (2H, s). The absence of the hydroxyl proton (-OH) signal in the NMR spectrum is likely due to rapid proton exchange with the solvent. ^{19}F NMR (DMSO-d_6) δ: −152.66 (4F, s), −159.29 (2F, s), −163.13 (4F, s).

Synthesis of p-t-BuL^{5}H

As for *p*-MeL^{1}H, but using pentafluoroaniline (1.78 g, 9.72 mmol) and 2,6-diformyl-4-*t*-butylphenol (1.00 g, 4.85 mmol) affording *p-t*-BuL^{5}H as a yellow solid. Crystallization from a saturated acetonitrile solution at ambient temperature afforded large yellow needle-shaped crystals. Yield: 1.94 g, 79%. Found C 53.84, H 2.41, N 5.23%. $C_{24}H_{14}N_2F_{10}O$ (sample dried *in vacuo* for 2 h) requires C 53.74, H 2.63, N 5.22%. IR: 3497w, 3404w, 1695m, 1665m, 1651m, 1616s, 1588s, 1510s, 1333m, 1311m, 1280s, 1226s, 1204m, 1171m, 1139s, 1123s, 1110s, 1073s, 1011s, 971s, 950s, 903m, 888m, 822s, 760m, 723s, 689w, 668w, 658w, 643w, 630w. Mass Spec (*m/z*): 575 (MK^+). ^{1}H NMR (DMSO-d_6) δ: 2.37 (9H, s), 7.90-8.29 (2H, m), 10.31 (2H, d, J = 44.7 Hz). The absence of the hydroxyl proton (-OH) signal in the NMR spectrum is likely due to rapid proton exchange with the solvent. ^{19}F NMR (DMSO-d_6) δ: −152.59 (4F, s), −159.14 (2F, s), −163.12 (4F, s).

Synthesis of p-MeL^{6}H

As for *p*-MeL[1]H but using 2-(trifluoromethyl)aniline (1.96 g (1.53 mL), 12.2 mmol) and 2,6-diformyl-4-methylphenol (1.00 g, 6.09 mmol) affording *p*-MeL[6]H as an orange solid. Crystallization from a saturated acetonitrile solution at ambient temperature afforded orange prisms. Yield: 2.00 g, 73%. Found C 60.99, H 3.51, N 6.17%. $C_{23}H_{16}N_2F_6O$ (sample dried *in vacuo* for 2 h) requires C 61.34, H 3.58, N 6.22%. IR: 2070w, 1966w, 1942w, 1933w, 1804w, 1676w, 1661s, 1594s, 1578s, 1317s, 1268s, 1231w, 1211s, 1206s, 1162s, 1109s, 1055s, 1032s, 981s, 951s, 929m, 893w, 879m, 862m, 857m, 811s, 802s, 779s, 765s, 748s, 723s, 673s, 647m, 642m. Mass Spec (*m/z*): 451 (MH^+). ^{1}H NMR (DMSO-d_6) δ: 2.38 (3H, s), 7.48 (2H, t, J = 7.6 Hz), 7.52 (2H, d, J = 7.9 Hz), 7.76 (2H, d, J = 7.8 Hz), 7.79 (2H, d, J = 7.3 Hz), 7.87 (2H, s), 8.97 (2H, s). The absence of the hydroxyl proton (-OH) signal in the NMR spectrum is likely due to rapid proton exchange with the solvent. ^{19}F NMR (DMSO-d_6) δ: −58.81 (6F, s).

Synthesis of p-t-BuL[6]H

As for *p*-MeL[1]H but using 2-(trifluoromethyl)aniline (1.57 g, 9.74 mmol) and 2,6-diformyl-4-*t*-butylphenol (1.00 g, 4.85 mmol) affording *p-t*-BuL[6]H as an orange solid. Crystallization from a saturated acetonitrile solution at ambient temperature afforded large orange prisms. Yield: 1.70 g, 71%. Found C 62.76, H 4.57, N 5.69%. $C_{26}H_{22}N_2F_6O$ (sample dried *in vacuo* for 2 h) requires C 63.41, H 4.50, N 5.69%. IR:.1961w, 1928w, 1825w, 1684w, 1625s, 1591s, 1578s, 1489s, 1319s, 1282m, 1268s, 1234m, 1214m, 1200m, 1164s, 1134s, 1112s, 1056s, 1035s, 1007m, 983m, 975m, 947w, 898w, 880w, 859w, 840w, 820w, 799w, 774s, 759s, 749s, 723s, 709m, 670w, 647w, 641w. Mass Spec (*m/z*): 493 (MH^+). ^{1}H NMR (DMSO-d_6) δ: 1.34 (9H, d, J = 10.2 Hz), 7.48 (2H, t, J = 7.6 Hz), 7.55 (2H, d, J = 7.9 Hz), 7.76 (2H, d, J = 7.8 Hz), 7.80 (2H, d, J = 7.4 Hz), 8.15 (2H, s), 9.03 (2H, s). The absence of the hydroxyl proton (-OH) signal in the NMR spectrum is likely due to rapid proton exchange with the solvent. ^{19}F NMR (DMSO-d_6) δ: −58.90 (6F, s).

Synthesis of p-MeL[7]H

As for *p*-MeL[1]H, but using 4-fluoro-2-iodoaniline (2.88 g, 12.2 mmol) and 2,6-diformyl-4-methylphenol (1.00 g, 6.09 mmol) affording *p*-MeL[7]H as a yellow solid. Crystallization from a saturated acetonitrile solution at ambient temperature afforded yellow prisms. Yield: 2.12 g, 58%. Found C 42.17, H 1.80, N 4.44%. $C_{21}H_{14}N_2F_2I_2O$ requires C 41.89, H 2.34, N 4.65%. IR: 1656w, 1625m, 1615m, 1594m, 1579m, 1324m, 1266s, 1253s, 1183s, 1160m, 1078w, 1044w, 1028m, 985w, 974m, 890w, 875m, 965w, 853m, 823m, 812s, 775m, 758m, 722s, 664w, 637w. Mass Spec (*m/z*): 603 (MH^+), 625 (MNa^+). ^{1}H NMR (DMSO-d_6) δ: 2.38 (3H, s), 7.41-7.35 (2H, m), 7.44 (2H, dd, J = 8.8, 5.5 Hz), 7.85 (2H, d, J = 2.7 Hz), 7.87 (2H, d, J = 4.1 Hz), 8.86 (2H, s). The absence of the hydroxyl proton (-OH) signal in the NMR spectrum is likely due to rapid proton exchange with the solvent. ^{19}F NMR (DMSO-d_6) δ: −115.40 (2F, s).

*Synthesis of p-t-*BuL[7]H

As for *p*-MeL[1]H, but using 4-fluoro-2-iodoaniline (2.31 g, 9.75 mmol) and 2,6-diformyl-4-*t*-butylphenol (1.00 g, 4.85 mmol) affording *p-t*-BuL[7]H as an orange solid. Crystallization from a saturated acetonitrile solution at ambient temperature afforded orange prisms. Yield: 2.43 g, 78%. Found C 44.65, H 3.87, N 4.44%. $C_{24}H_{20}N_2F_2I_2O$ requires C 44.74, H 3.13, N 4.35%. IR: 1634s, 1607m, 1522s, 1480s, 1370m, 1333s, 1304w, 1269m, 1238m, 1185s, 1130w, 900w, 864s, 820w, 797w, 659m, 599w, 563w. Mass Spec (*m/z*): 645 (MH^+), 667 (MNa^+). ^{1}H NMR (DMSO-d_6) δ: 1.36 (9H, s), 7.39 (2H, td, J = 8.5, 2.8 Hz), 7.46 (2H, dd, J = 8.9, 5.4 Hz), 7.86 (2H, dd, J = 8.1, 2.8 Hz), 8.16 (2H, s), 8.91 (2H, s). The absence of the hydroxyl proton (-OH) signal in the NMR spectrum is likely due to rapid proton exchange with the solvent. ^{19}F NMR (DMSO-d_6) δ: −115.38 (2F, s).

Table S1. Crystallographic data of *p*-MeL[3]H, *p*-MeL[5]H, **1**, and **3**.

Compound	*p*-MeL[3]H	*p*-MeL[5]H	**1**	**3**
Formula	$C_{29}H_{34}N_2O$	$C_{21}H_8F_{10}N_2O$	$C_{50}H_{50}N_4O_3V$	$C_{56}H_{82}N_4VO_3$
Formula weight	426.58	494.29	805.88	1030.29
Crystal system	Triclinic	Monoclinic	Monoclinic	Monoclinic
Space group	$P\bar{1}$	$P2_1/c$	$P2_1/n$	$P2_1/c$

Unit cell dimensions				
a (Å)	10.4654(2)	21.1845(7)	8.39860(10)	9.2637(5)
b (Å)	14.8091(2)	5.03630(10)	22.0578(3)	32.1121(19)
c (Å)	16.8078(3)	19.2407(7)	11.60800(10)	10.5093(6)
α (°)	74.785(2)	90	90	90
β (°)	81.0860(10)	116.974(4)	96.2020(10)	104.6408(10)
γ (°)	80.4970(10)	90	90	90
V (Å^3)	2462.01(8)	1829.56(11)	2137.85(4)	3024.8(3)
Z	4	4	2	2
Temperature (K)	100(2)	100(2)	99.99(10)	150(2)
Wavelength (Å)	1.54184	1.54178	1.54178	0.71073
Calculated density (g.cm^{-3})	1.151	1.795	1.252	1.131
Absorption coefficient (mm^{-1})	0.533	1.645	2.304	0.21
Transmission factors (min./max.)	0.901, 0.983	0.659, 1.000	0.780, 1.000	0.884, 0.963
Crystal size (mm^3)	0.21 × 0.16 × 0.03	0.20 × 0.02 × 0.01	0.12 × 0.07 × 0.03	0.60 × 0.58 × 0.18
θ(max) (°)	154.02	147.33	150.24	25.0
Reflections measured	47699	31527	25035	21743
Unique reflections	9932	3642	4275	5325
R_{int}	0.055	0.051	0.026	0.036
Reflections with $F^2 > 2\sigma(F^2)$				4311
Number of parameters	593	315	351	352
R_1 [$F^2 > 2\sigma(F^2)$]	0.0461	0.0409	0.0359	0.127
wR_2 (all data)	0.1299	0.1215	0.1046	0.315
GOOF, S	1.04	1.058	1.04	1.18
Largest difference peak and hole (e Å^{-3})	0.31 and –0.24	0.27 and –0.25	0.23 and –0.26	0.58 and –0.52

Table S2. Crystallographic data of **11**, **12**, **12′**, and **14**.

Compound	**11**	**12**·toluene	**12′**·1.5MeCN	**14**·MeCN
Formula	$C_{46}H_{30}N_4VO_3{\cdot}C_2H_3N$	$C_{52}H_{42}F_{12}N_4VO_3{\cdot}$toluene	$C_{52}H_{42}F_{12}N_4VO_3{\cdot}1.5C_2H_3N$	$C_{48}H_{38}F_4I_4N_4O_3V{\cdot}C_2H_3N$
Formula weight	1006.73	1141.97	1111.41	1394.42
Crystal system	Triclinic	Monoclinic	Monoclinic	Triclinic
Space group	$P\ \bar{1}$	$C2/c$	$P2_1/n$	$P\ \bar{1}$
Unit cell dimensions				
a (Å)	12.19953(12)	34.8959(7)	18.5994(10)	11.4085(3)
b (Å)	14.8420(2)	10.6717(3)	12.4821(7)	13.1317(4)
c (Å)	26.2894(2)	30.5882(7)	23.4986(7)	17.4790(4)

α (°)	93.4728(9)	90	90	78.084(2)
β (°)	99.0009(8)	109.452(2)	99.056(5)	86.776(2)
γ (°)	106.4579(10)	90	90	89.036(3)
V (Å^3)	4481.12(9)	10740.8(5)	5387.4(6)	2558.06(12)
Z	4	8	4	2
Temperature (K)	100(2)	100(2)	100(2)	100(2)
Wavelength (Å)	1.54178	1.54184	1.54184	1.54178
Calculated density (g.cm^{-3})	1.492	1.412	1.370	1.810
Absorption coefficient (mm^{-1})	2.73	2.34	2.325	21.08
Transmission factors (min./max.)	0.931, 1.000	0.248, 1.000	0.976, 0.997	0.579, 1.000
Crystal size (mm^3)	0.12 × 0.07 × 0.04	0.34 × 0.19 × 0.11	0.17 × 0.10 × 0.05	0.14 × 0.11 × 0.04
θ(max) (°)	73.8	150.65	107.1	70.2
Reflections measured	142364	50560	27764	46832
Unique reflections	17015	10685	6373	9620
R_{int}	0.035	0.067	0.117	0.060
Reflections with $F^2 > 2\sigma(F^2)$	15992	7629	8654	7851
Number of parameters	1249	719	672	611
R_1 [$F^2 > 2\sigma(F^2)$]	0.069	0.052	0.092	0.057
wR_2 (all data)	0.202	0.151	0.723	0.159
GOOF, S	1.17	1.07	1.04	1.05
Largest difference peak and hole (e Å^{-3})	1.48 and –0.47	1.10 and –0.47	0.57 and –0.65	2.18 and –1.55

Table S3. Details of C=N bond lengths in free ligands and metal complexes.

Compound	Unbound C=N lengths / Å	Mean / Å	Bound C=N lengths / Å	Mean / Å
pMeL3H	1.2820(17), 1.2775(16), 1.2826(17), 1.2738(17)	1.279, σ=0.004		
pMeL5H	1.287(2), 1.285(2)	1.286		
1	1.2696(17)		1.2864(16)	
3	1.266(7)		1.286(6)	
11	1.275(4), 1.269(5), 1.269(5), 1.277(4)	1.273, σ=0.004	1.284(5), 1.298(5), 1.289(4), 1.299(5)	1.293, σ=0.007
12	1.273(3), 1.268(3)	1.271	1.292(3), 1.298(3)	1.295
14	1.265(8), 1.267(9)	1.266	1.296(8), 1.296(8)	1.296

σ is the standard deviation of the set of bond lengths where more than two bond lengths are present.

All structures were determined at 100K except for **3** which was studied at 150K.

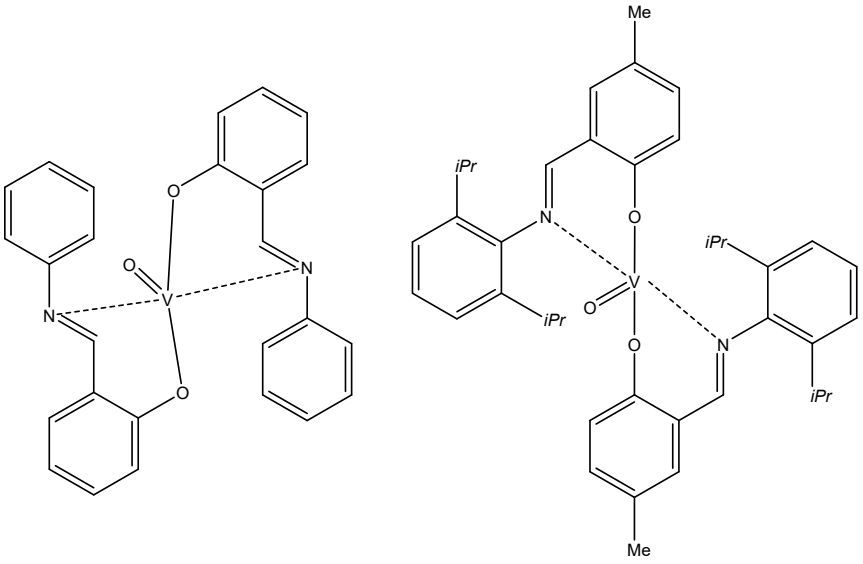

R1 **R2**

Chart S1. The structures of **R1** and **R2**.

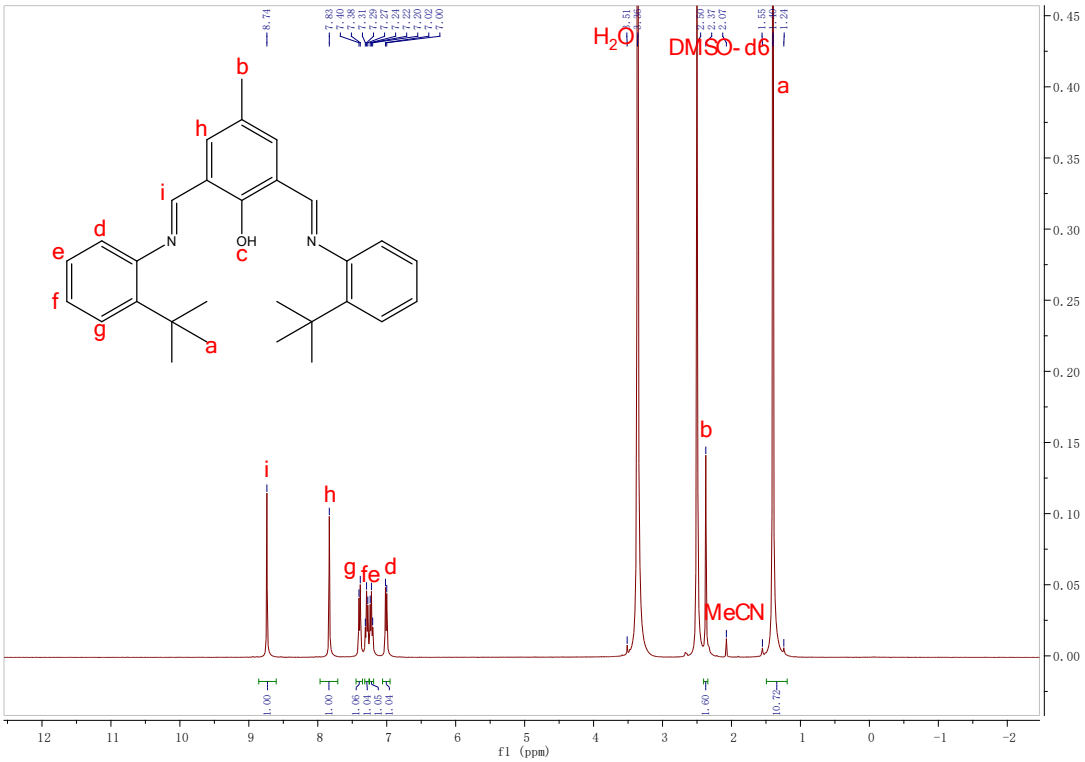

Figure S1. ^{1}H NMR spectrum of *p*-MeL^{3}H in DMSO-d$_6$ at 298 K.

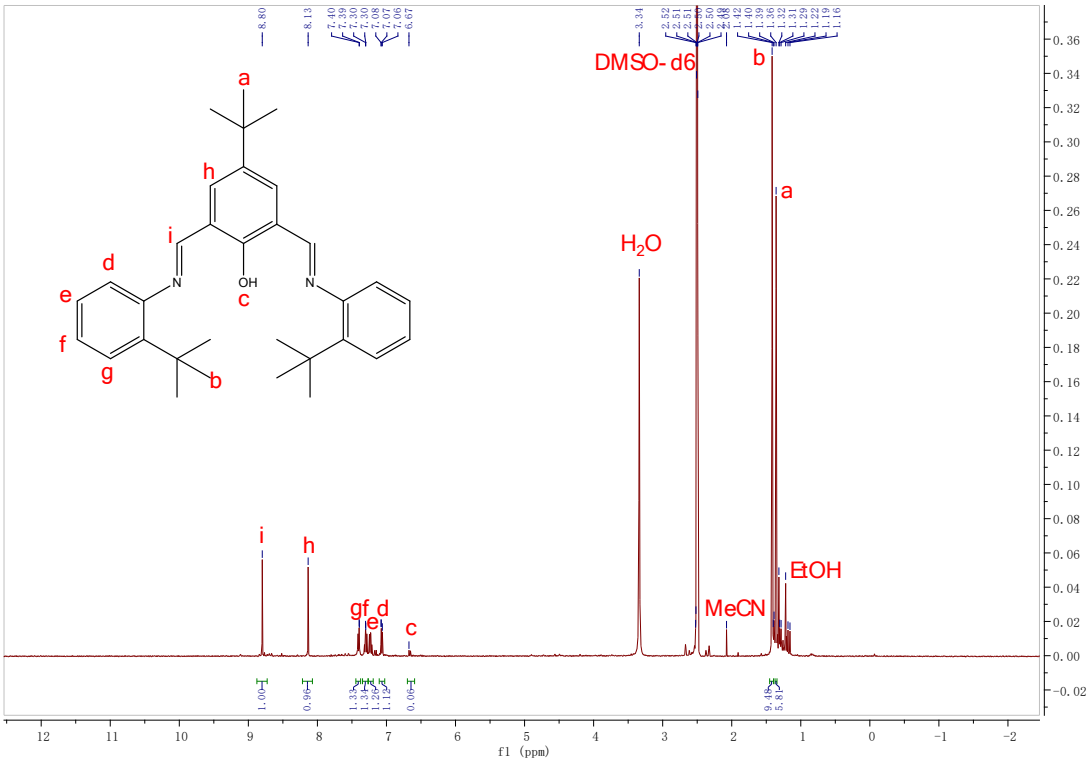

Figure S2. ^{1}H NMR spectrum of *p*-*t*-BuL^{3}H in DMSO-d$_6$ at 298 K.

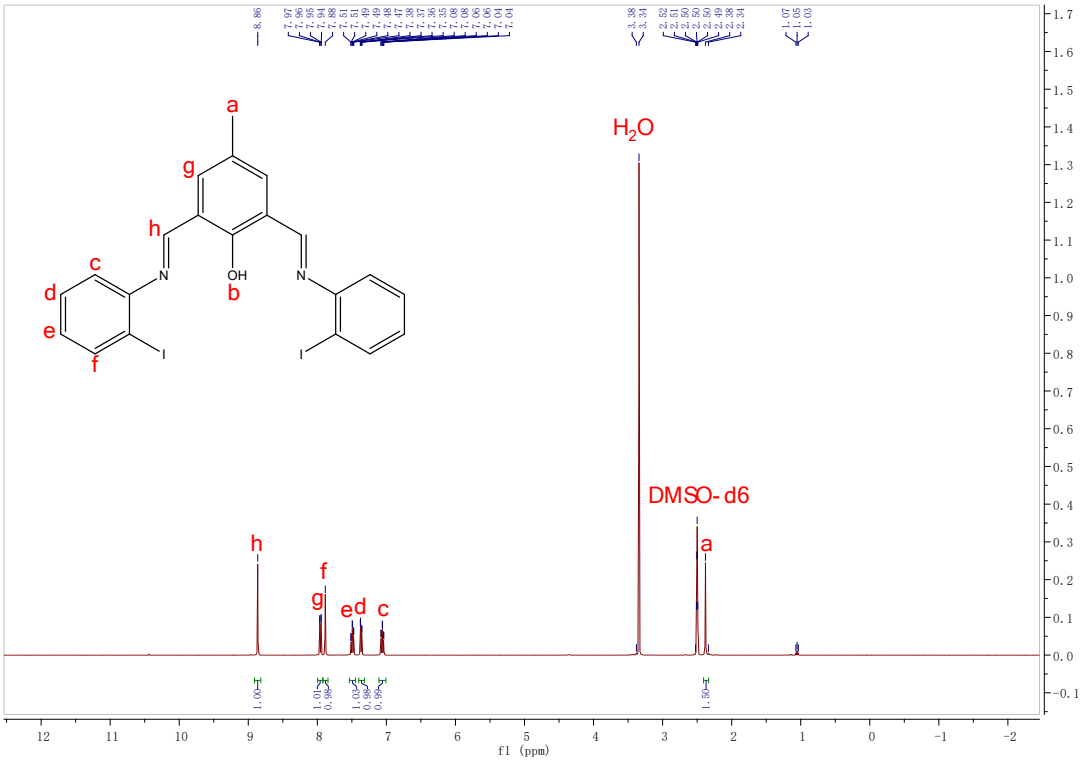

Figure S3. ^{1}H NMR spectrum of *p*-MeL^{4}H in DMSO-d$_6$ at 298 K.

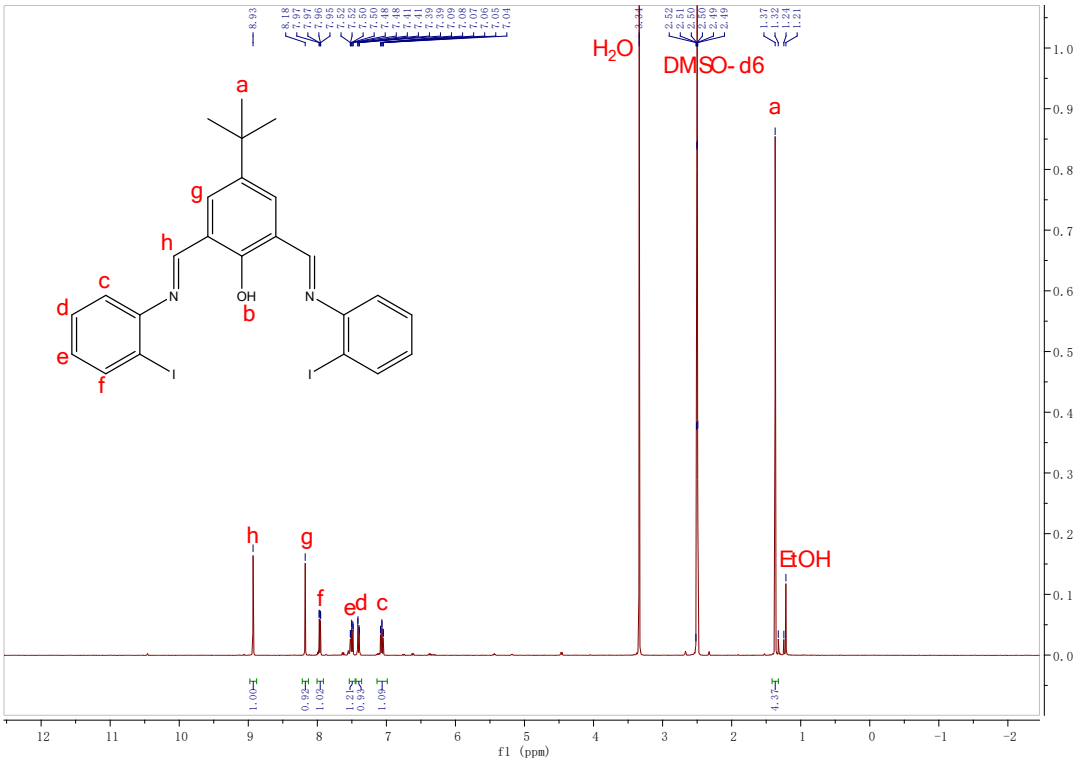

Figure S4. ^{1}H NMR spectrum of *p*-*t*-BuL^{4}H in DMSO-d_6 at 298 K.

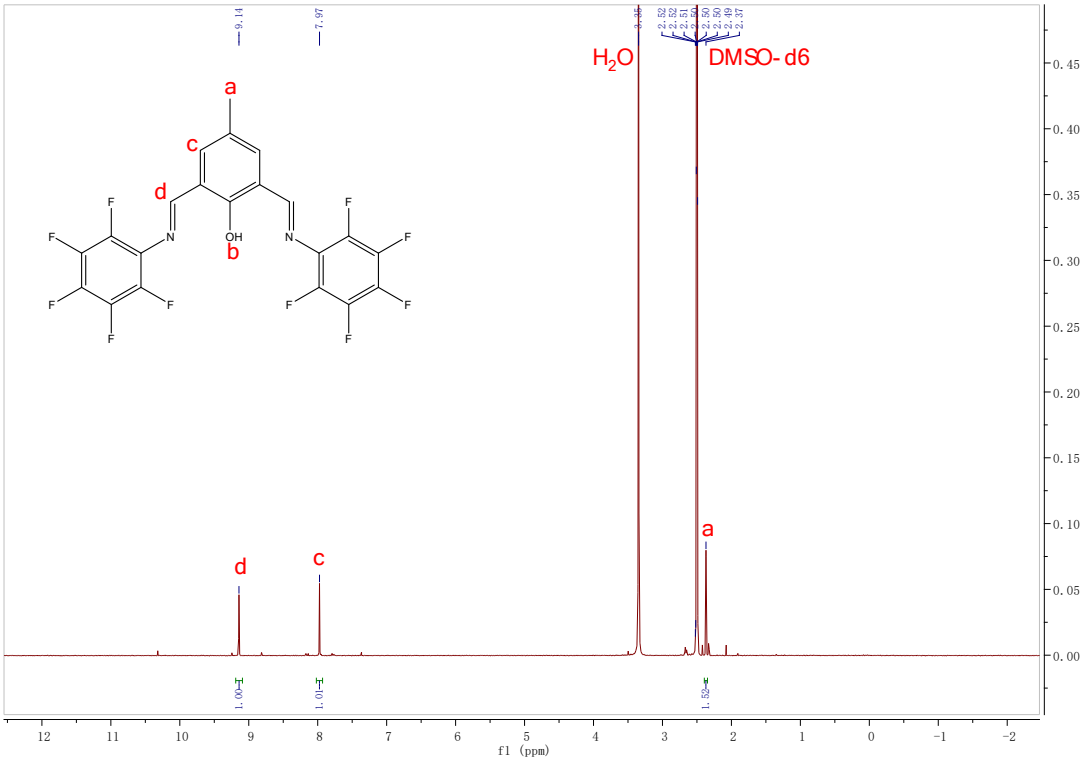

Figure S5. ^{1}H NMR spectrum of *p*-MeL^{5}H in DMSO-d_6 at 298 K.

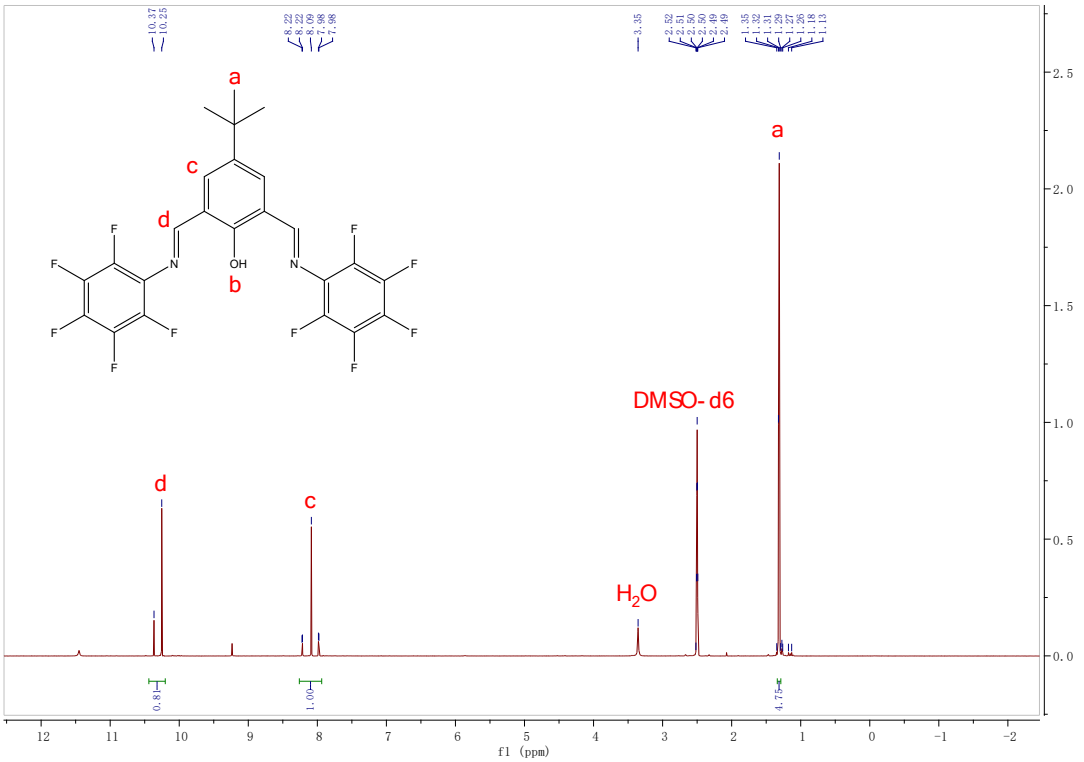

Figure S6. ^{1}H NMR spectrum of *p*-*t*-BuL^{5}H in DMSO-d_6 at 298 K.

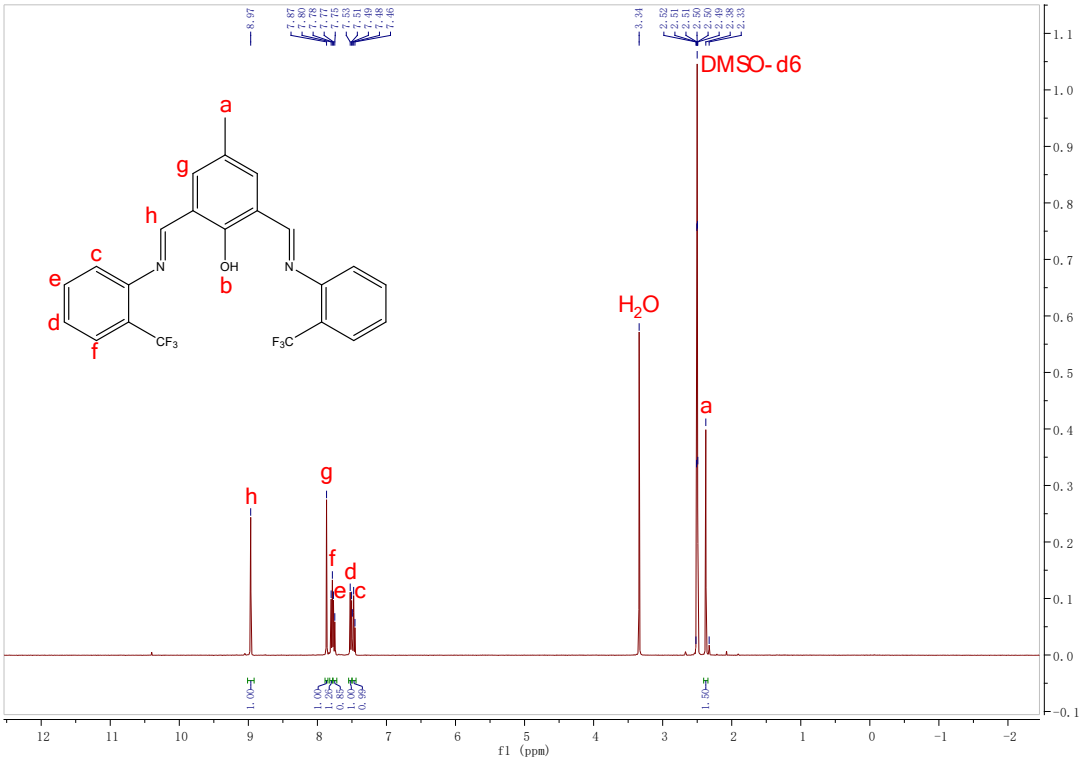

Figure S7. ^{1}H NMR spectrum of *p*-MeL^{6}H in DMSO-d_6 at 298 K.

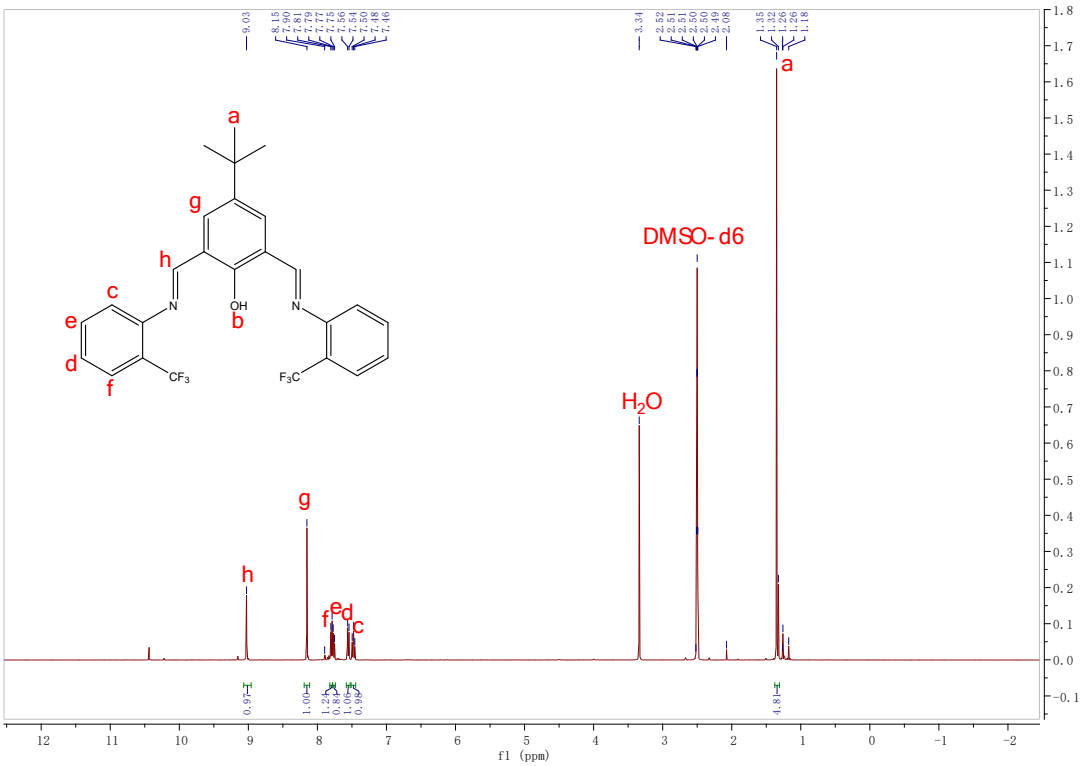

Figure S8. ^{1}H NMR spectrum of *p*-*t*-BuL^{6}H in DMSO-d$_6$ at 298 K.

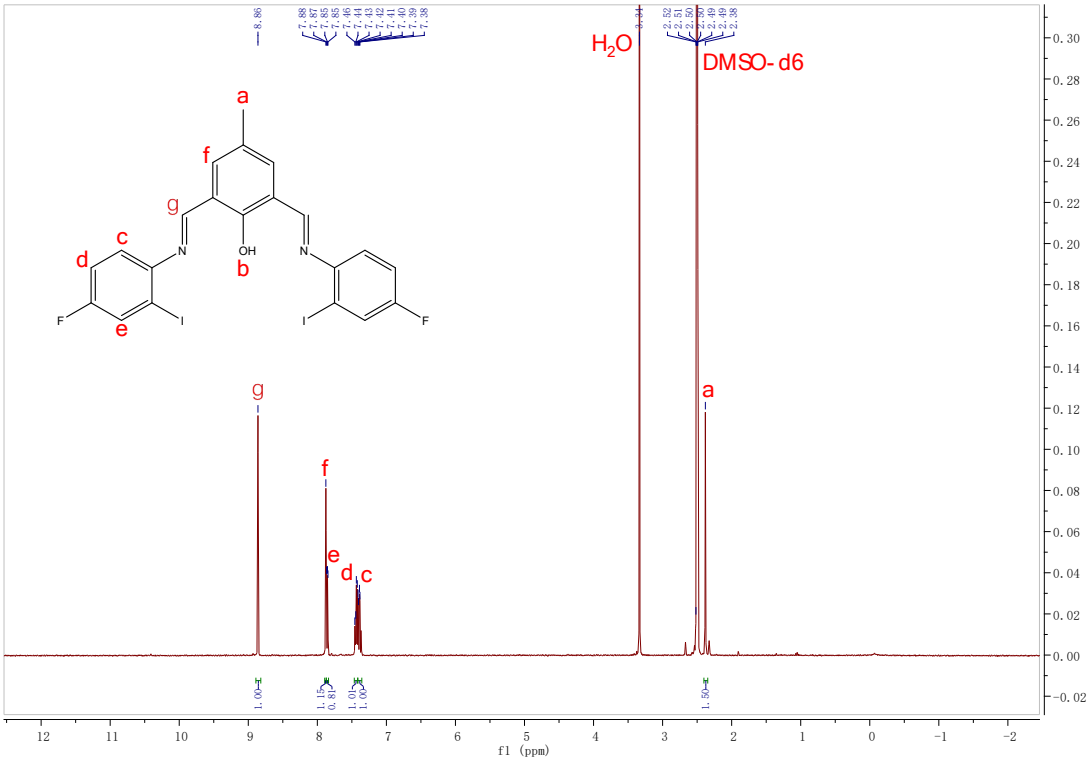

Figure S9. ^{1}H NMR spectrum of *p*-MeL^{7}H in DMSO-d$_6$ at 298 K.

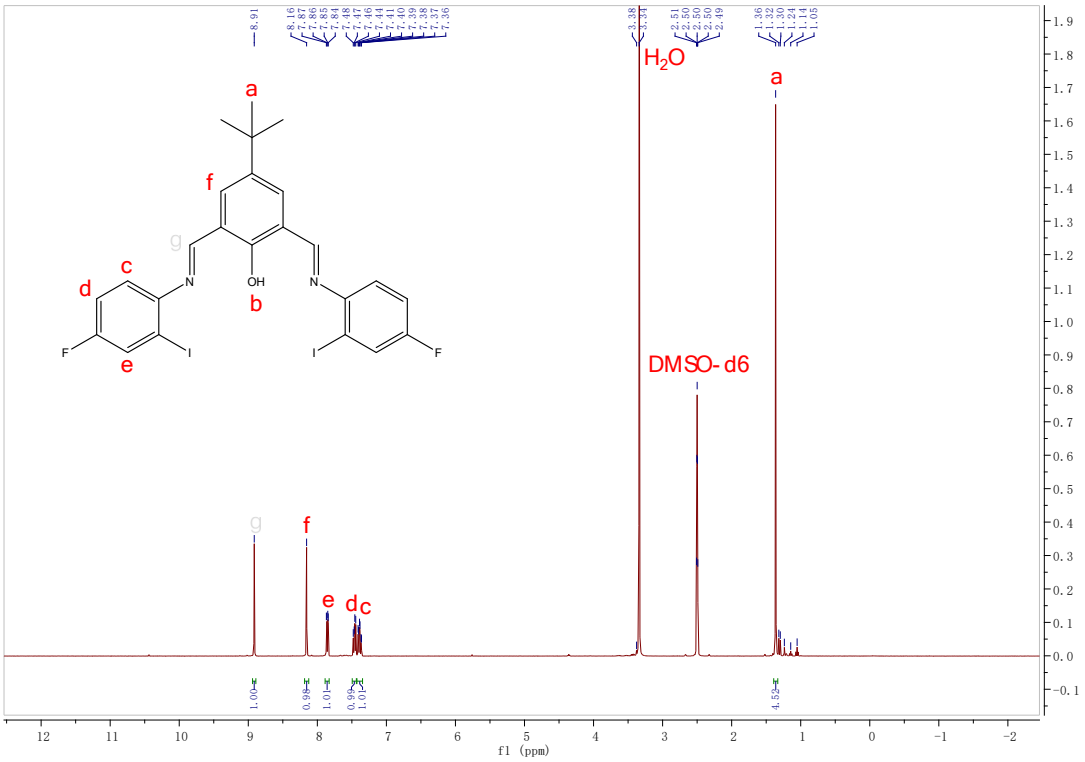

Figure S10. ^{1}H NMR spectrum of *p*-*t*-BuL^{7}H in DMSO-d$_6$ at 298 K.

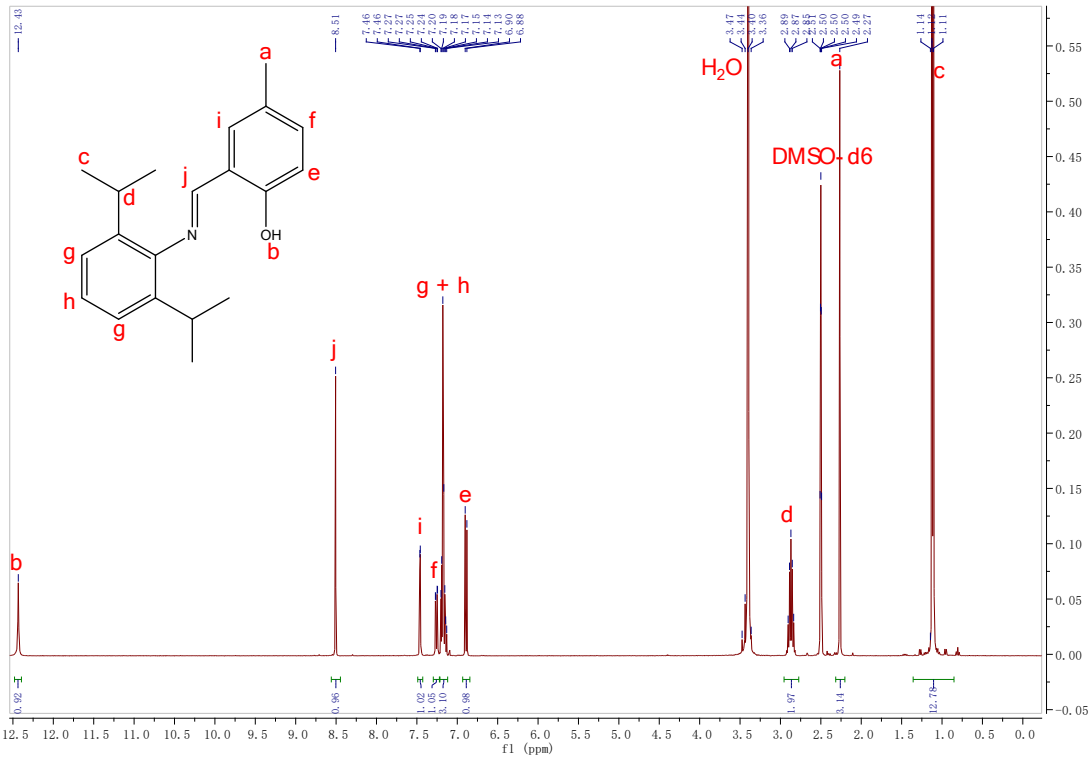

Figure S11. ^{1}H NMR spectrum of **R2**-L in DMSO-d$_6$ at 298 K.

Table S4. Results for ROP of ε-CL in toluene over 24h using **1** – **14** and **I**.

Entry	Cat.	[CL]:[Cat]:[BnOH]	T(°C)	Conv[a] (%)	$M_{n\ obs}$[b]	$M_{n,Calc}$[c]	$Đ$[d]
S1	**1**	500:1:0	15	0	-	-	-
S2[e]	**1**	500:1:0	15	0	-	-	-
S3	**1**	500:1:1	15	0	-	-	-
S4[e]	**1**	500:1:1	15	0	-	-	-
S5	**1**	500:1:0	130	8	-	-	-
S6[e]	**1**	500:1:0	130	11	700	6280	1.23
S7	**2**	500:1:0	130	62	6280	35380	1.97
S8[e]	**2**	500:1:0	130	98	6070	55930	2.13
S9	**3**	500:1:0	130	10	-	-	-
S10[e]	**3**	500:1:0	130	98	6260	55930	2.06
S11	**4**	500:1:0	130	60	5050	34240	1.24
S12[e]	**4**	500:1:0	130	98	5770	55930	2.08
S13	**5**	500:1:0	130	55	3450	31390	1.48
S14[e]	**5**	500:1:0	130	98	7440	55930	1.71
S15	**6**	500:1:0	130	98	9760	55930	1.95
S16[e]	**6**	500:1:0	130	98	3440	55930	1.86
S17	**7**	500:1:0	130	17	4230	9700	1.47
S18[e]	**7**	500:1:0	130	83	4770	47370	1.73
S19	**8**	500:1:0	130	6	-	-	-
S20[e]	**8**	500:1:0	130	43	6000	24560	1.27
S21	**9**	500:1:0	130	3	-	-	-
S22[e]	**9**	500:1:0	130	38	5860	21710	1.27
S23	**10**	500:1:0	130	79	6130	45090	2.03
S24[e]	**10**	500:1:0	130	99	10400	56500	2.33
S25	**11**	500:1:0	130	43	6090	24540	1.42
S26[e]	**11**	500:1:0	130	85	7630	48510	1.85
S27	**12**	500:1:0	130	42	6650	23970	1.62
S28[e]	**12**	500:1:0	130	100	5920	57070	2.35
S29	**13**	500:1:0	130	13	3800	7420	1.27
S30[e]	**13**	500:1:0	130	95	7240	54220	1.73
S31	**14**	500:1:0	130	4	-	-	-
S32[e]	**14**	500:1:0	130	100	8830	57070	2.42
S33	**R1**	500:1:0	130	44	12620	25110	1.72
S34[e]	**R1**	500:1:0	130	84	7210	47940	2.87
S35	**R2**	500:1:0	130	38	8680	21690	1.46
S36[e]	**R2**	500:1:0	130	98	15830	55930	2.51
S37	**I**	500:1	130	0	-	-	-
S38[e]	**I**	500:1	130	12	2650	6850	1.70

[a] Conversion was confirmed by ^{1}H NMR spectroscopy. [b] GPC analysis in THF at ambient temperature, and polystyrene standards were used to calibrate the results (corrected by a factor [S3] of 0.56). [c] $M_{n,calc} = M_0$x([CL]/[Cat])xconversion + $M_{end\ group}$. [d] Polydispersity index (M_w/M_n) was calculated by GPC. [e] Conducted in air.

Table S5. Synthesis of polycaprolactone using complexes **1** – **14** (and **I**) as melts (130 °C, 24 h).

Entry	Cat.	[CL]:[Cat]:[BnOH]	Conv[a] (%)[a]	$M_{n,obs}$[b]	$M_{n,calc}$[c]	$Đ$[d]
S1	**1**	500:1:0	9	-	-	-
S2[e]	**1**	500:1:0	94	9020	53650	2.26
S3	**1**	500:1:1	71	7770	40630	1.49
S4[e]	**1**	500:1:1	48	2700	27500	2.69
S5	**2**	500:1:0	65	4150	37100	2.65
S6[e]	**2**	500:1:0	99	9110	56500	1.74
S7	**3**	500:1:0	60	5890	34240	2.05
S8[e]	**3**	500:1:0	83	5060	47370	1.97
S9	**4**	500:1:0	43	10460	24540	2.70
S10[e]	**4**	500:1:0	78	9000	44510	1.82
S11	**5**	500:1:0	85	9910	48510	2.42
S12[e]	**5**	500:1:0	71	9360	40520	1.97
S13	**6**	500:1:0	56	7350	31960	1.85
S14[e]	**6**	500:1:0	95	8890	54220	2.12
S15	**7**	500:1:0	0	-	-	-
S16[e]	**7**	500:1:0	50	7610	28540	2.35
S17	**8**	500:1:0	73	8910	41660	1.55
S18[e]	**8**	500:1:0	73	7180	41660	2.61
S19	**9**	500:1:0	86	10800	49080	1.92
S20[e]	**9**	500:1:0	77	9150	43940	2.33
S21	**10**	500:1:0	79	11650	45090	2.24
S22[e]	**10**	500:1:0	75	7500	42800	2.04
S23	**11**	500:1:0	63	8020	35950	2.51
S24[e]	**11**	500:1:0	99	8140	56500	2.39
S25	**12**	500:1:0	86	10010	49080	1.86
S26[e]	**12**	500:1:0	85	7480	48510	1.58
S27	**13**	500:1:0	99	6030	56500	1.82
S28[e]	**13**	500:1:0	95	9950	54220	2.35
S29	**14**	500:1:0	99	7700	56500	1.79
S30[e]	**14**	500:1:0	100	7960	57070	2.10
S31	**R1**	500:1:0	98	18300	55930	3.65
S32[e]	**R1**	500:1:0	100	7080	57070	2.75
S33	**R2**	500:1:0	81	4470	46230	2.68
S34[e]	**R2**	500:1:0	100	8650	57070	2.61
S35	**I**	500:1:0	56	3950	31960	1.47
S36[e]	**I**	500:1:0	6	-	-	-

[a] Conversion was confirmed by ^{1}H NMR spectroscopy. [b] GPC analysis in THF at ambient temperature, and polystyrene standards were used to calibrate the results (corrected by a factor [S3] of 0.56). [c] $M_{n,calc} = M_0$x([CL]/[Cat])xconversion + $M_{end\ group}$. [d] Polydispersity index (M_w/M_n) was calculated by GPC. [e] Conducted in air

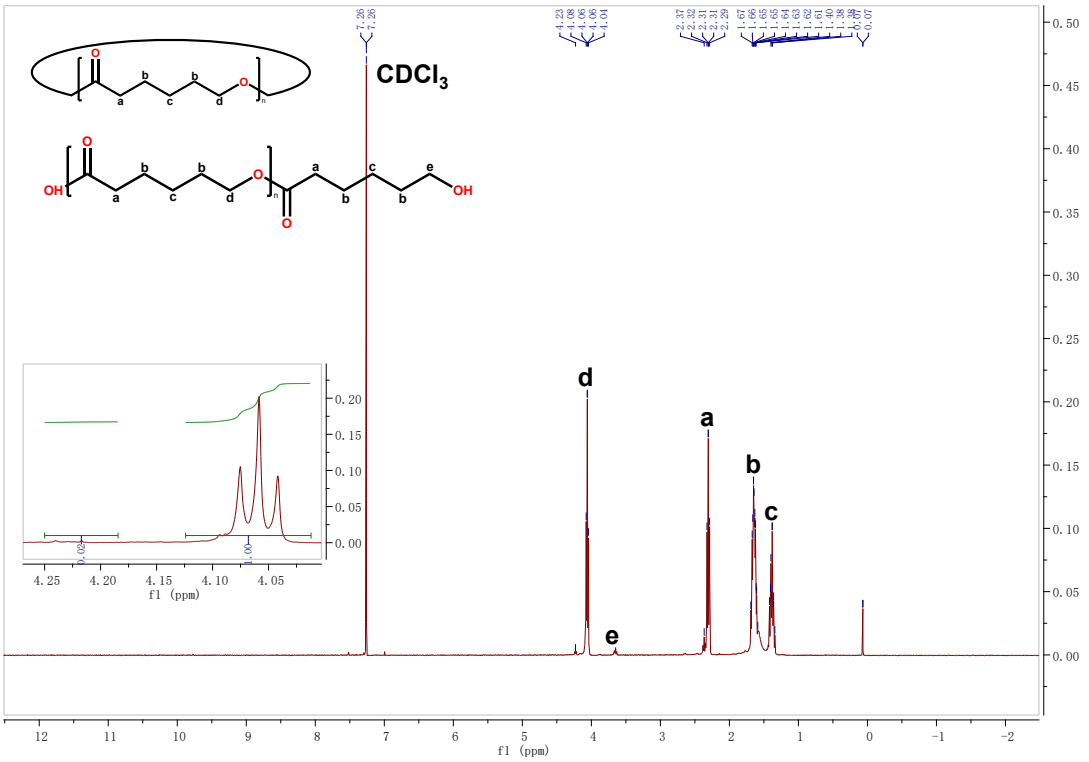

Figure S12. ^{1}H NMR spectrum of PCL in $CDCl_3$ at 298 K (Table 1, entry 3; Table S1, entry S8).

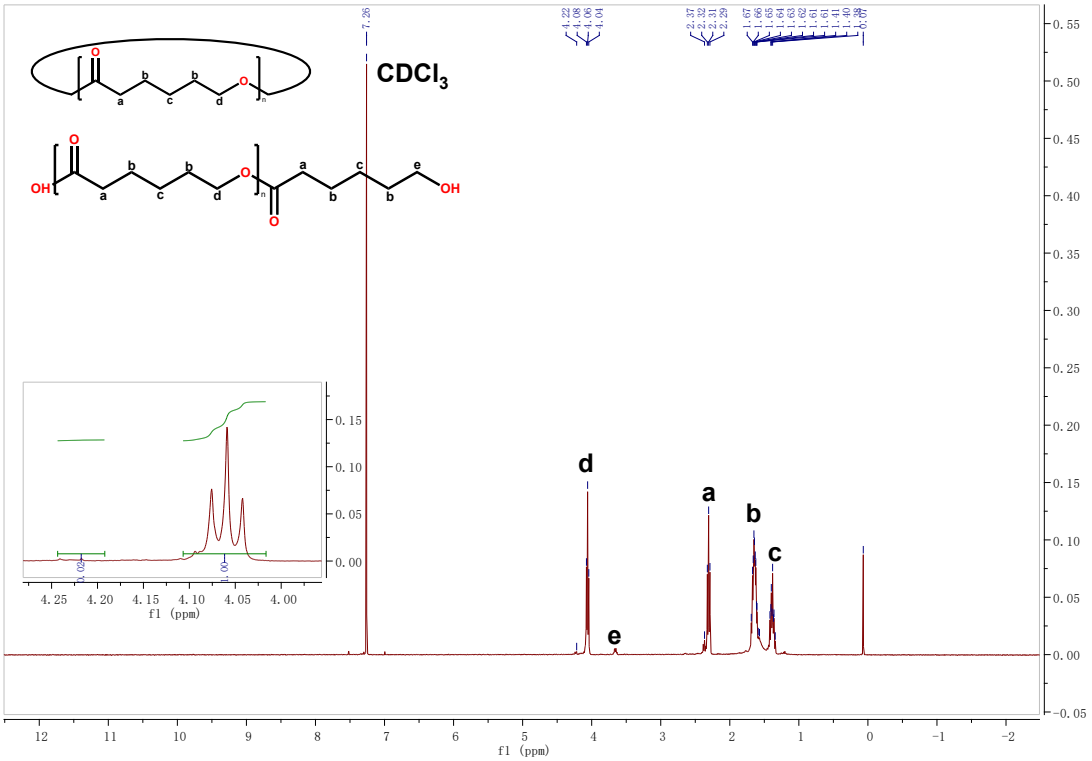

Figure S13. ^{1}H NMR spectrum of PCL in $CDCl_3$ at 298 K (Table 1, entry 5; Table S1, entry S10).

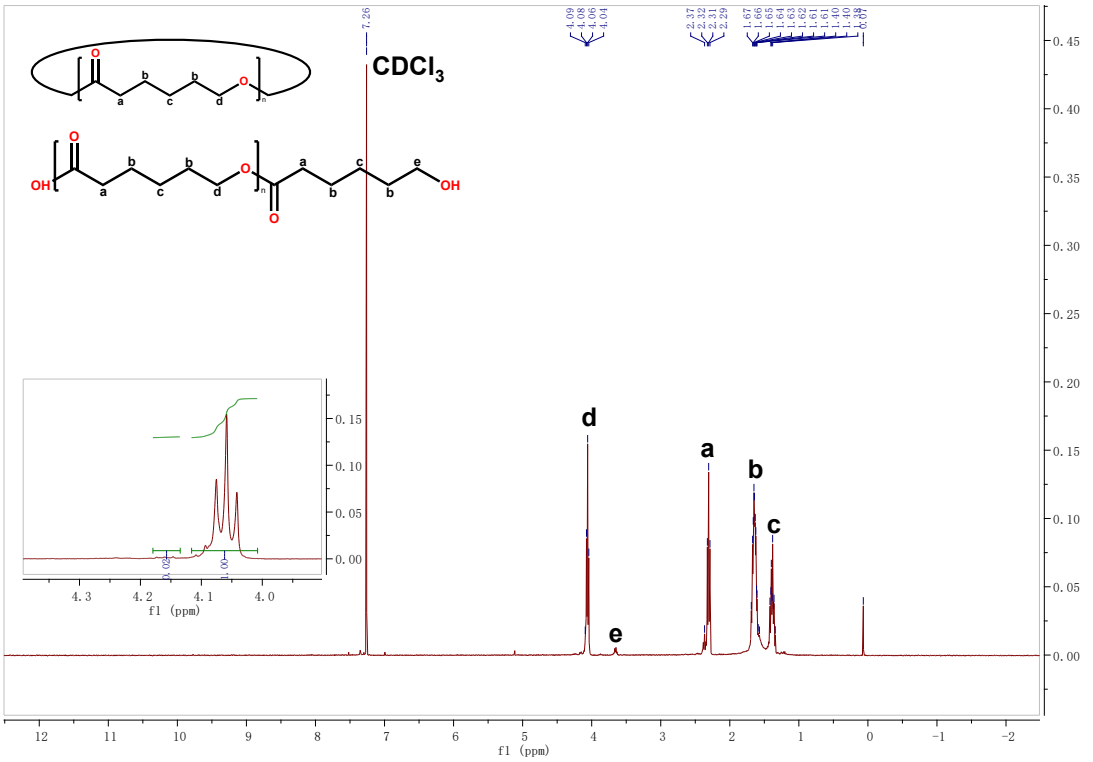

Figure S14. ^{1}H NMR spectrum of PCL in $CDCl_3$ at 298 K (Table S1, entry S12).

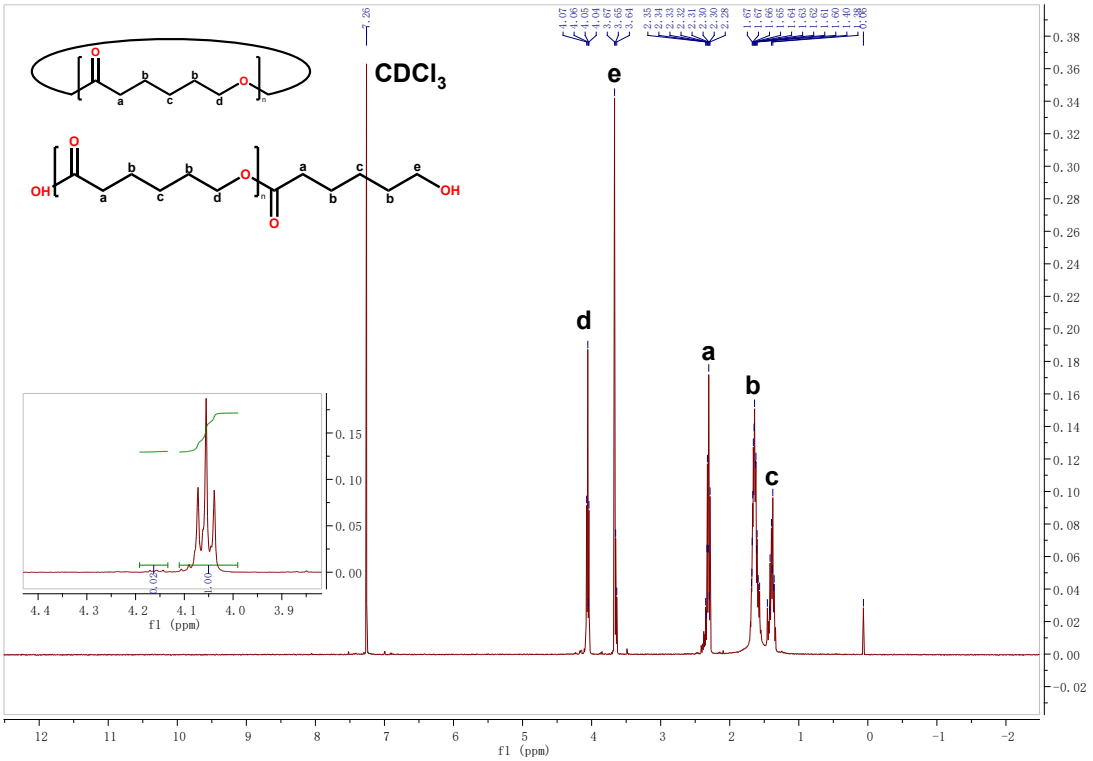

Figure S15. ^{1}H NMR spectrum of PCL in $CDCl_3$ at 298 K (Table 1, entry 7; Table S1, entry S14).

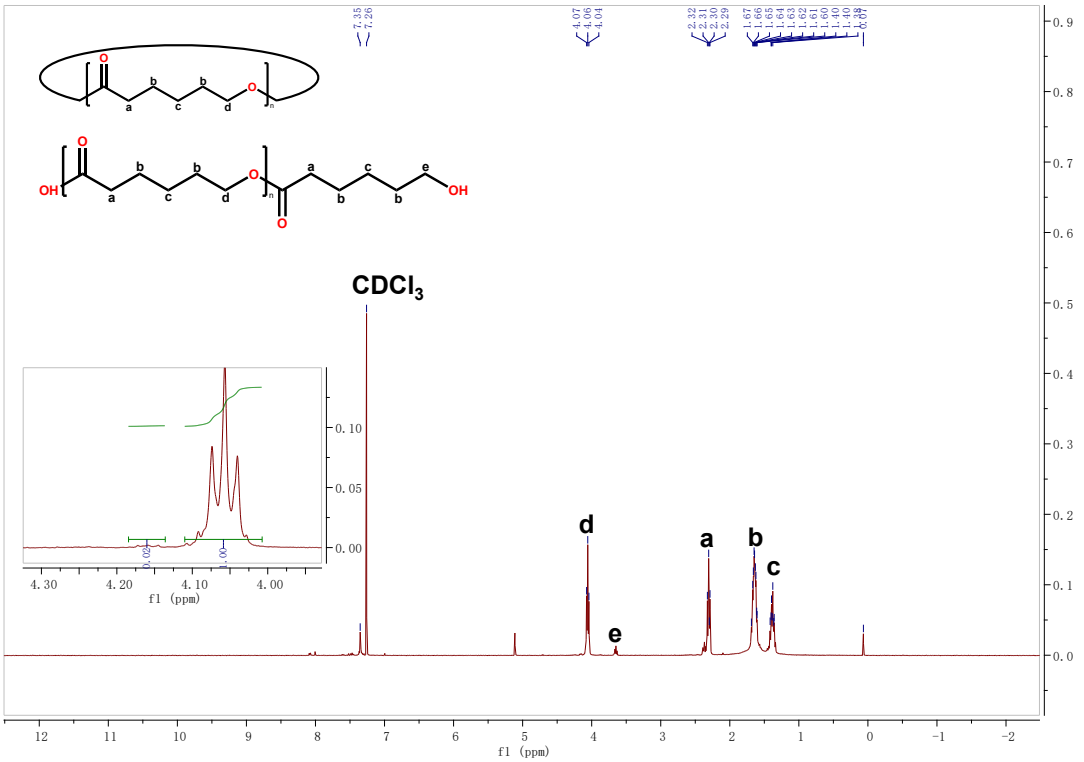

Figure S16. ^{1}H NMR spectrum of PCL in $CDCl_3$ at 298 K (Table S1, entry S16).

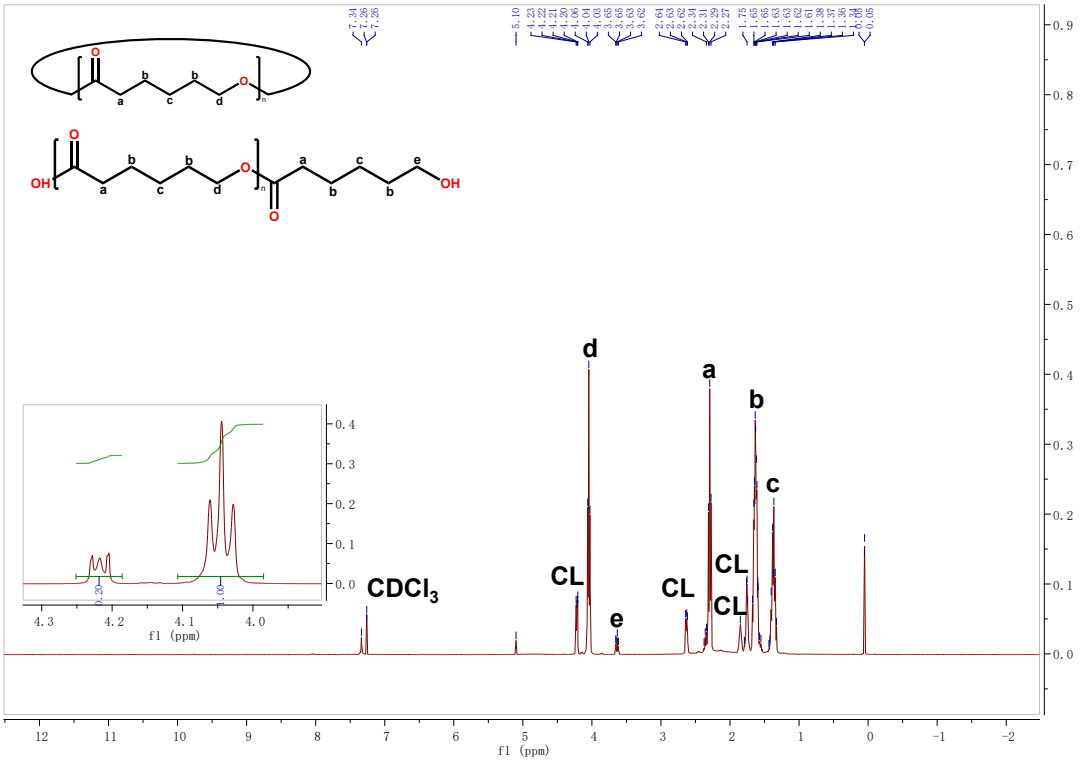

Figure S17. ^{1}H NMR spectrum of PCL in $CDCl_3$ at 298 K (Table S1, entry S18).

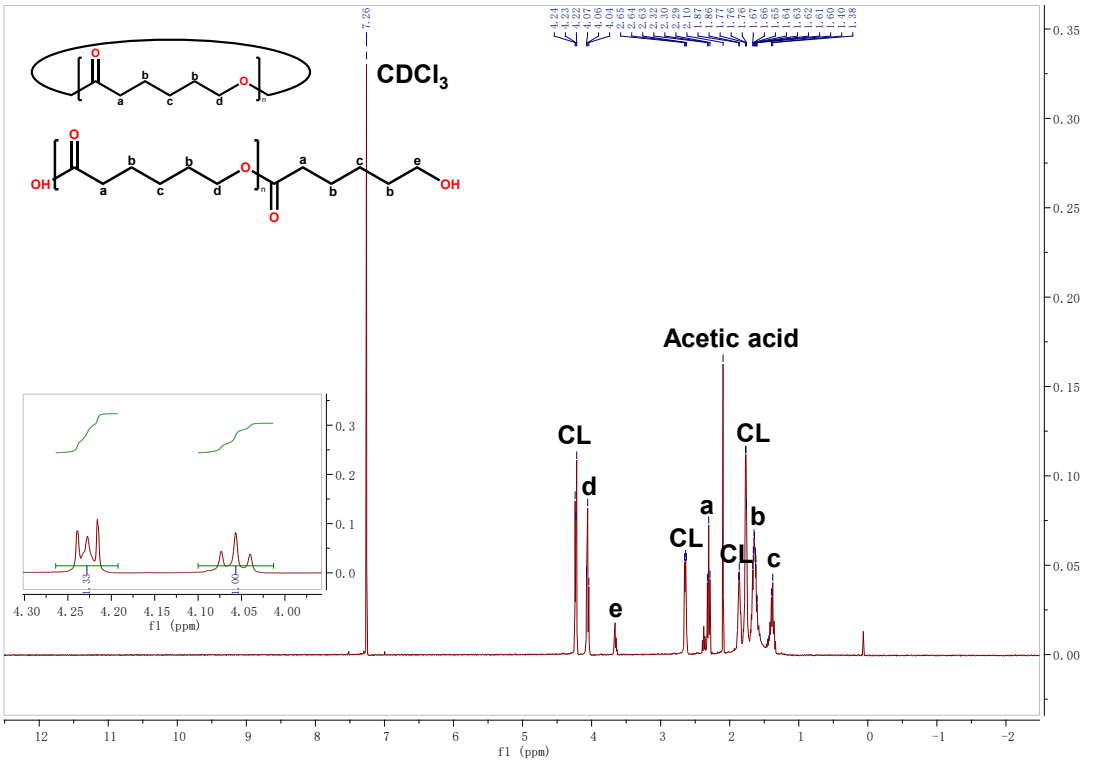

Figure S18. ^{1}H NMR spectrum of PCL in $CDCl_3$ at 298 K (Table 1, entry 10, Table S1, entry S20).

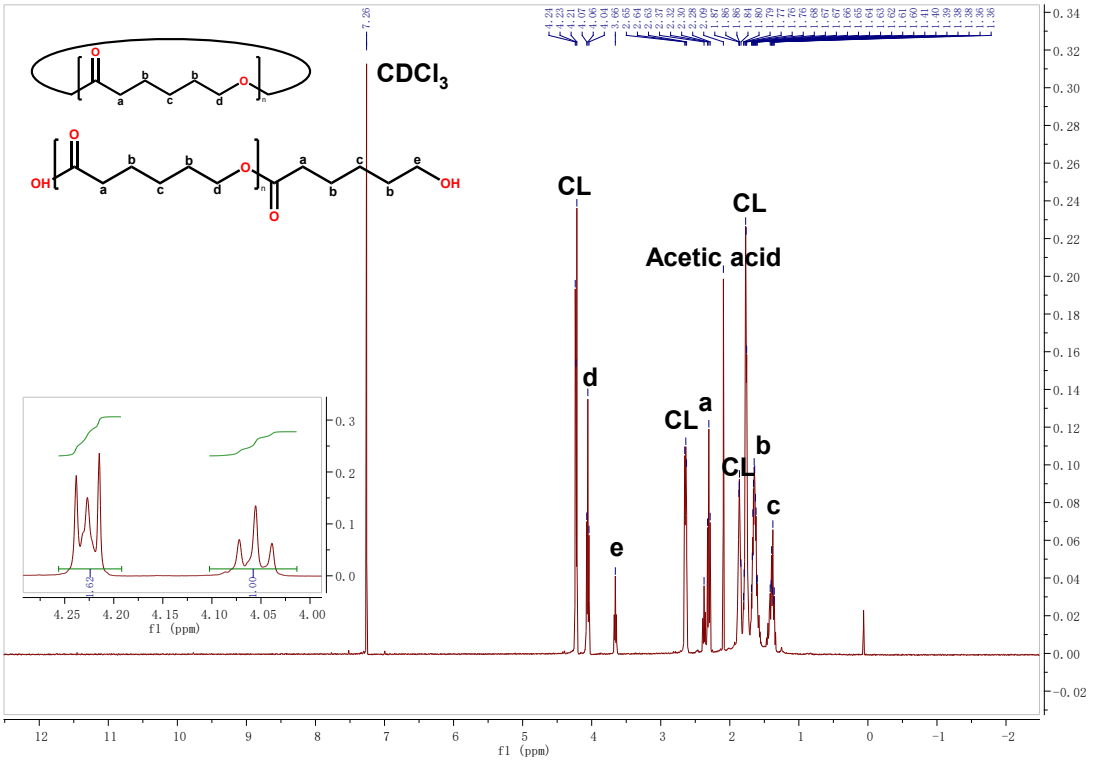

Figure S19. ^{1}H NMR spectrum of PCL in $CDCl_3$ at 298 K (Table 1, entry 11; Table S1, entry S22).

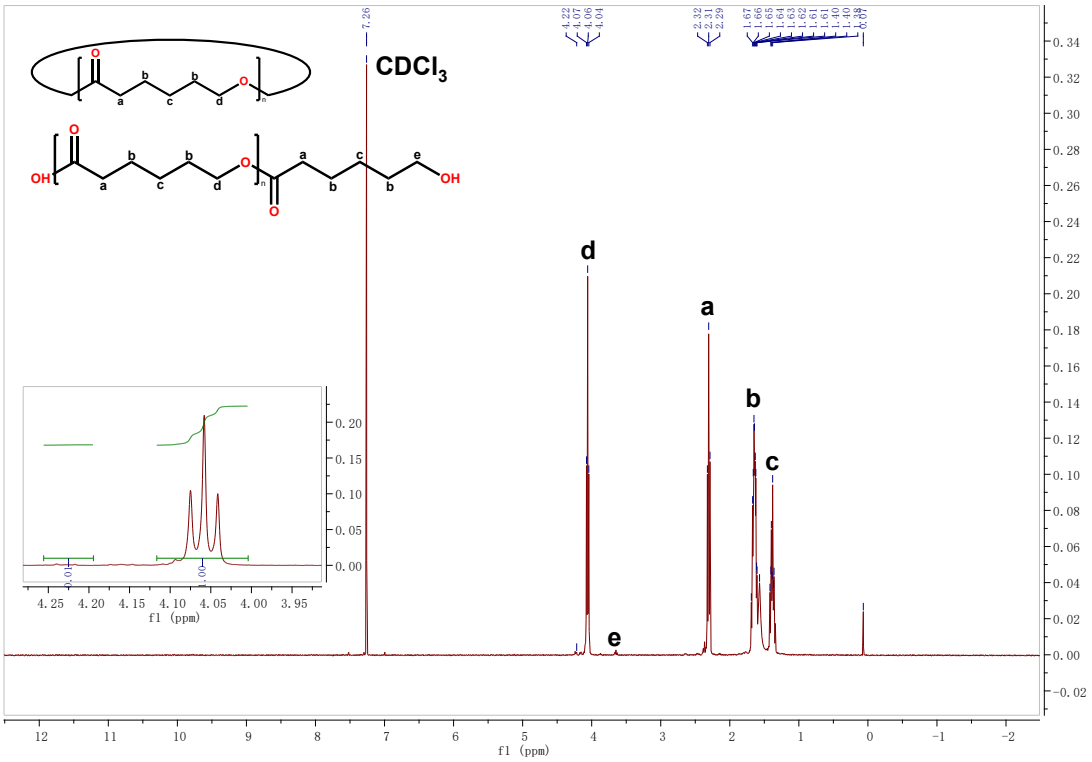

Figure S20. ^{1}H NMR spectrum of PCL in $CDCl_3$ at 298 K (Table 1, entry 12; Table S1, entry S24).

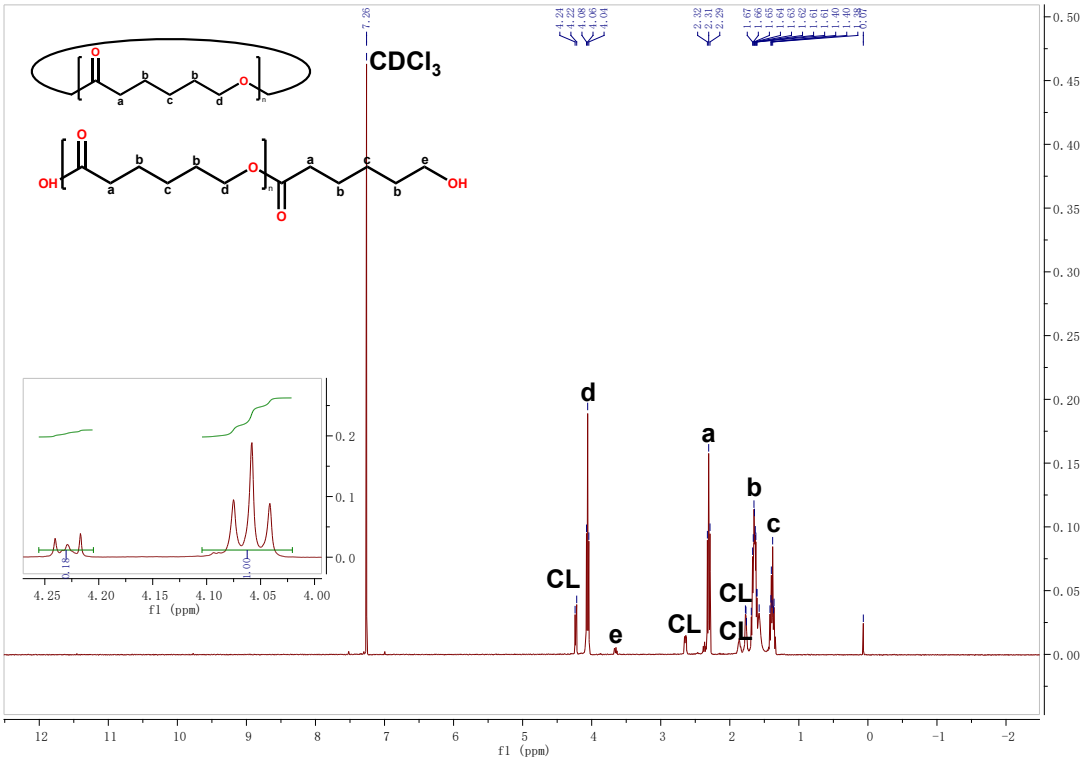

Figure S21. ^{1}H NMR spectrum of PCL in $CDCl_3$ at 298 K (Table S1, entry S26).

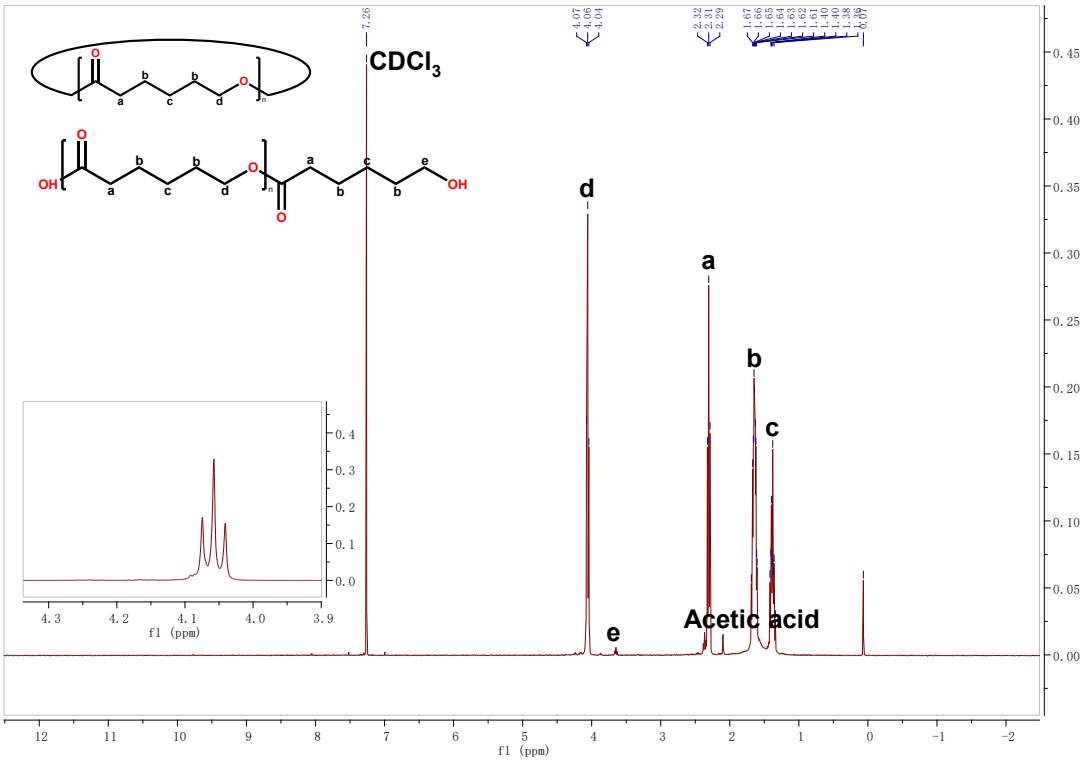

Figure S22. ^{1}H NMR spectrum of PCL in $CDCl_3$ at 298 K (Table S1, entry S28).

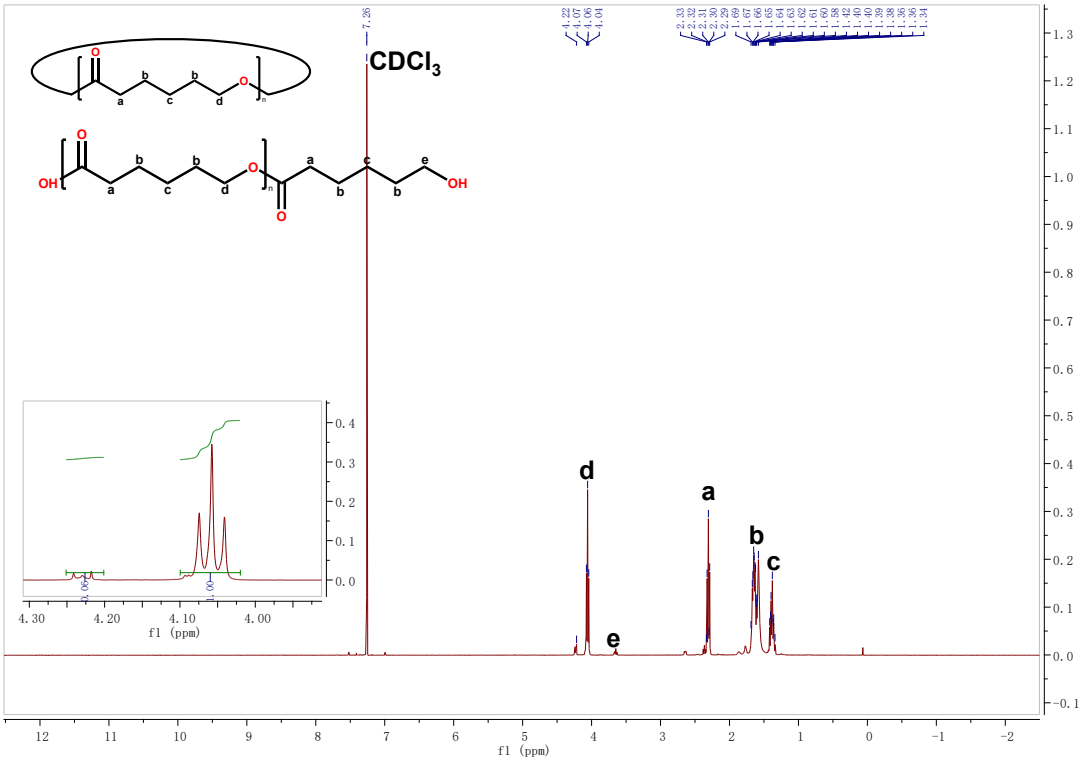

Figure S23. ^{1}H NMR spectrum of PCL in $CDCl_3$ at 298 K (Table S1, entry S30).

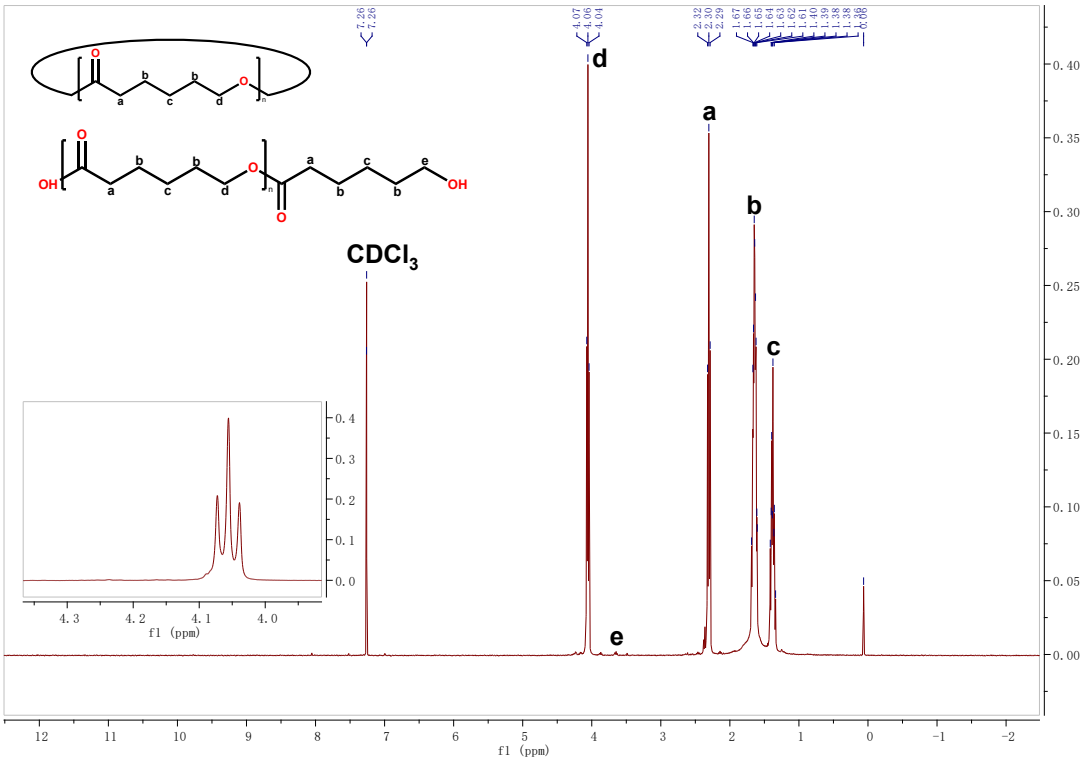

Figure S24. ^{1}H NMR spectrum of PCL in $CDCl_3$ at 298 K (Table 1, entry 16; Table S1, entry S32).

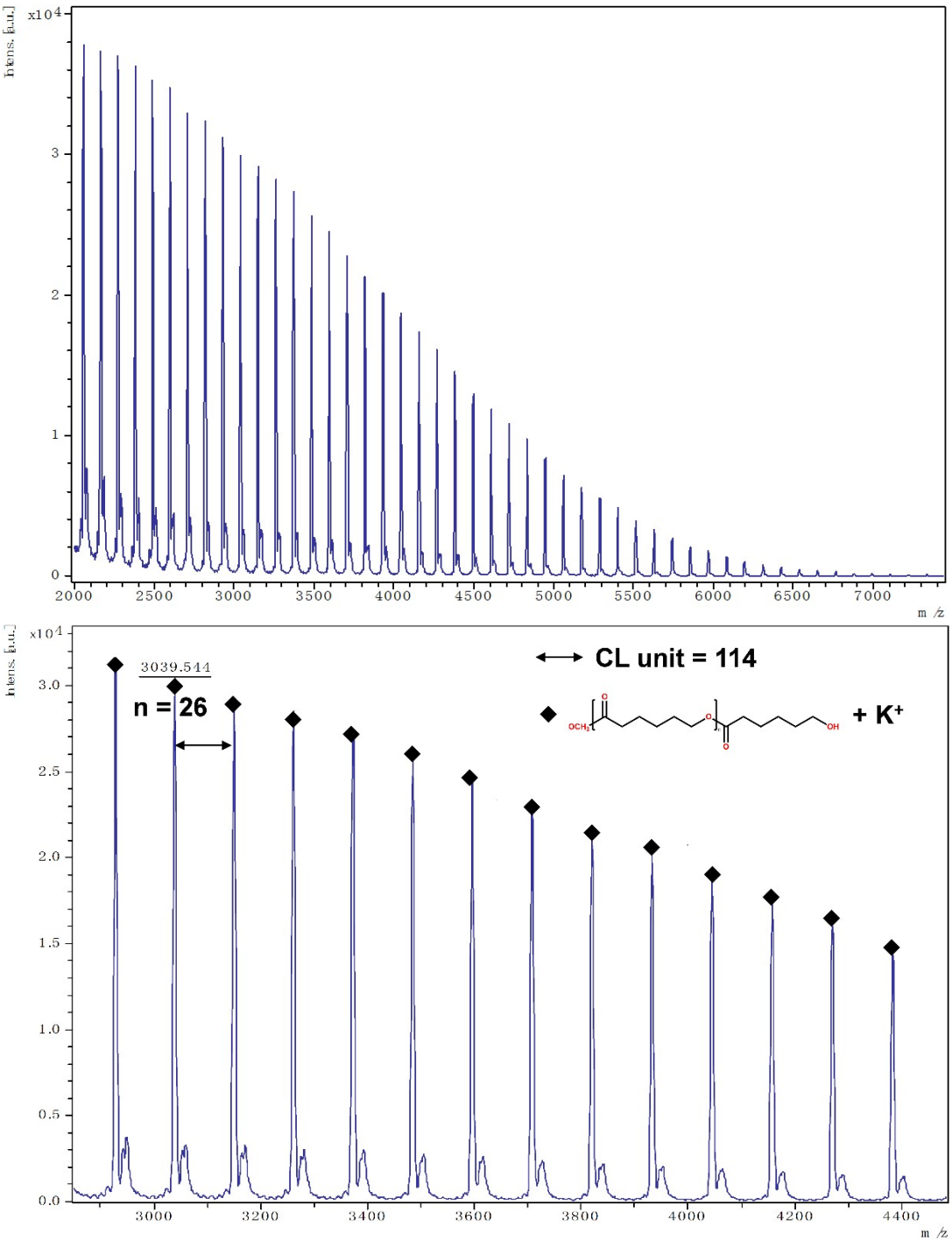

Figure S25. MALDI-TOF mass spectrum of PCL (Table 1, entry 3; Table S1; entry S8). The peak at *m/z* 3039.544 represents the linear PCL $H_3CO(CL)_nH$ with K^+ (*m/z*: 114.1 x n + 32.0 + 39.1, n = 26).

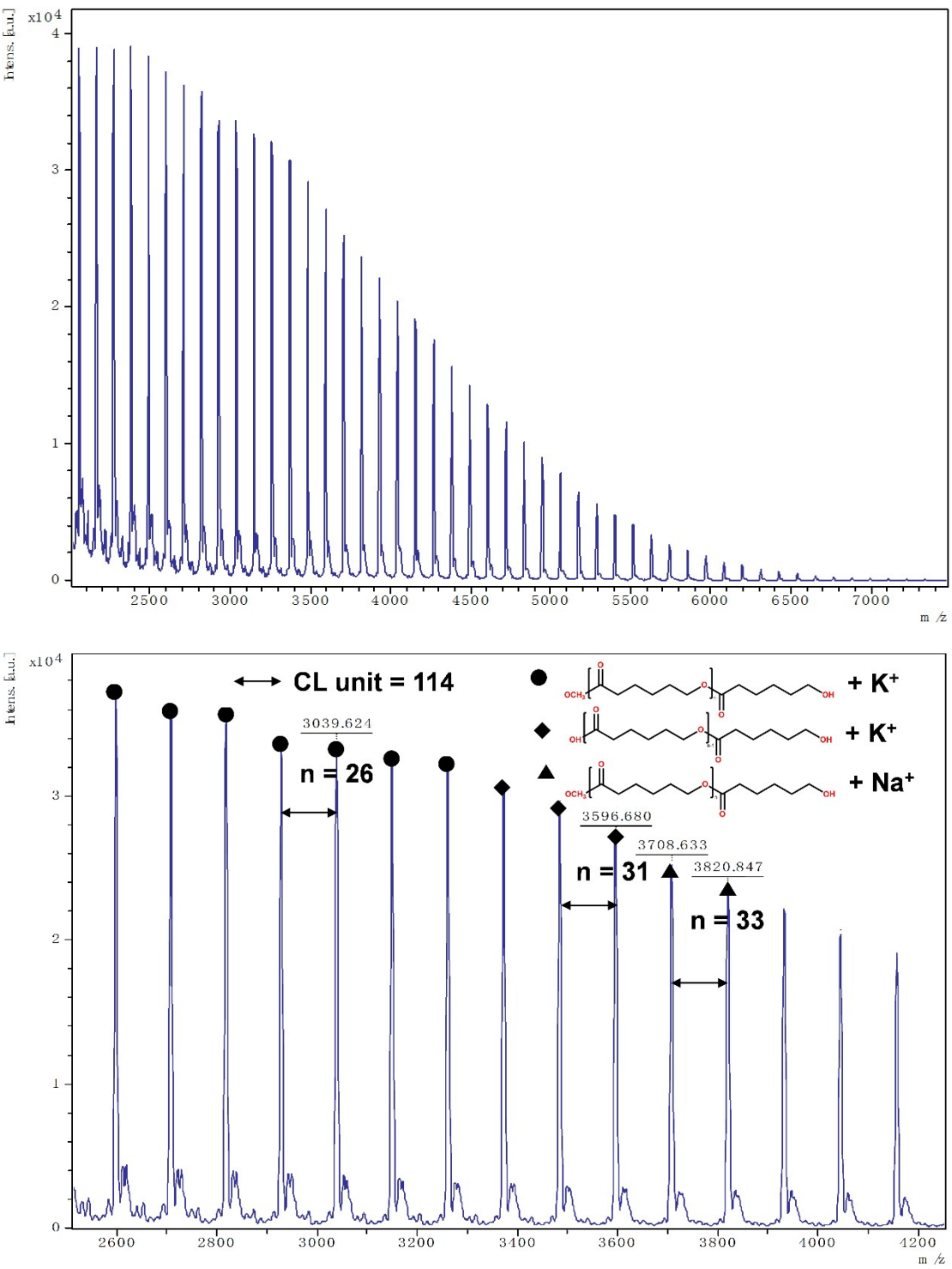

Figure S26. MALDI-TOF mass spectrum of PCL (Table 1, entry 5; Table S1, entry S10). The peak at *m/z* 3039.624 represents the linear PCL $H_3CO(CL)_nH$ with K^+ (*m/z*: 114.1 x n + 32.0 + 39.1, n = 26), the peak at *m/z* 3596.680 the linear PCL $HO(CL)_nH$ with K^+ (*m/z*: 114.1 x n + 18.0 + 39.1, n = 31), the peak at *m/z* 3820.847 represents the linear PCL $H_3CO(CL)_nH$ with Na^+ (*m/z*: 114.1 x n + 32.0 + 23.0, n = 33).

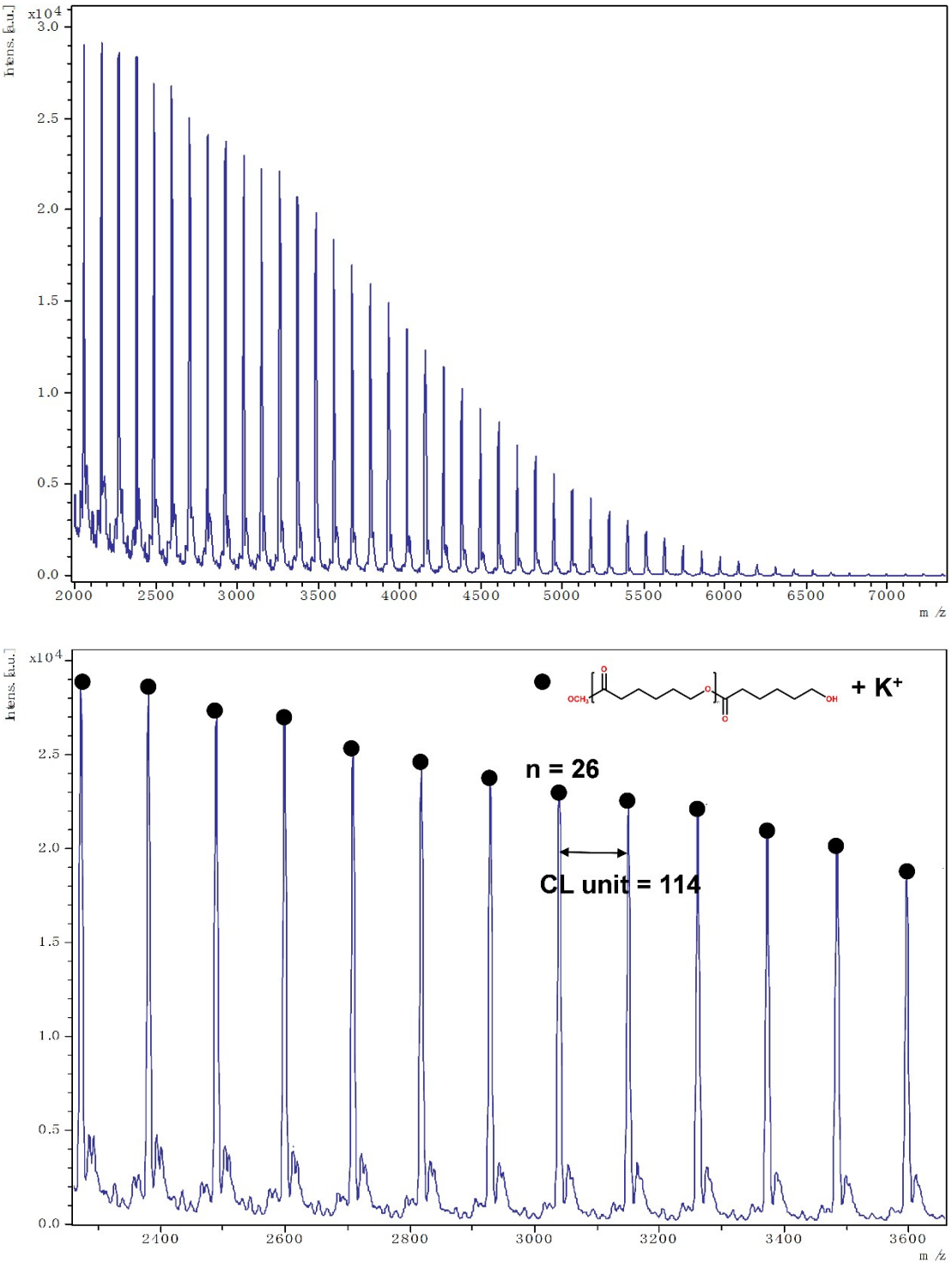

Figure S27. MALDI-TOF mass spectrum of PCL (Table S1; entry S12). The peak at *m/z* 3039.703 represents the linear PCL $H_3CO(CL)_nH$ with K^+ (*m/z*: 114.1 x n + 32.0 + 39.1, n = 26).

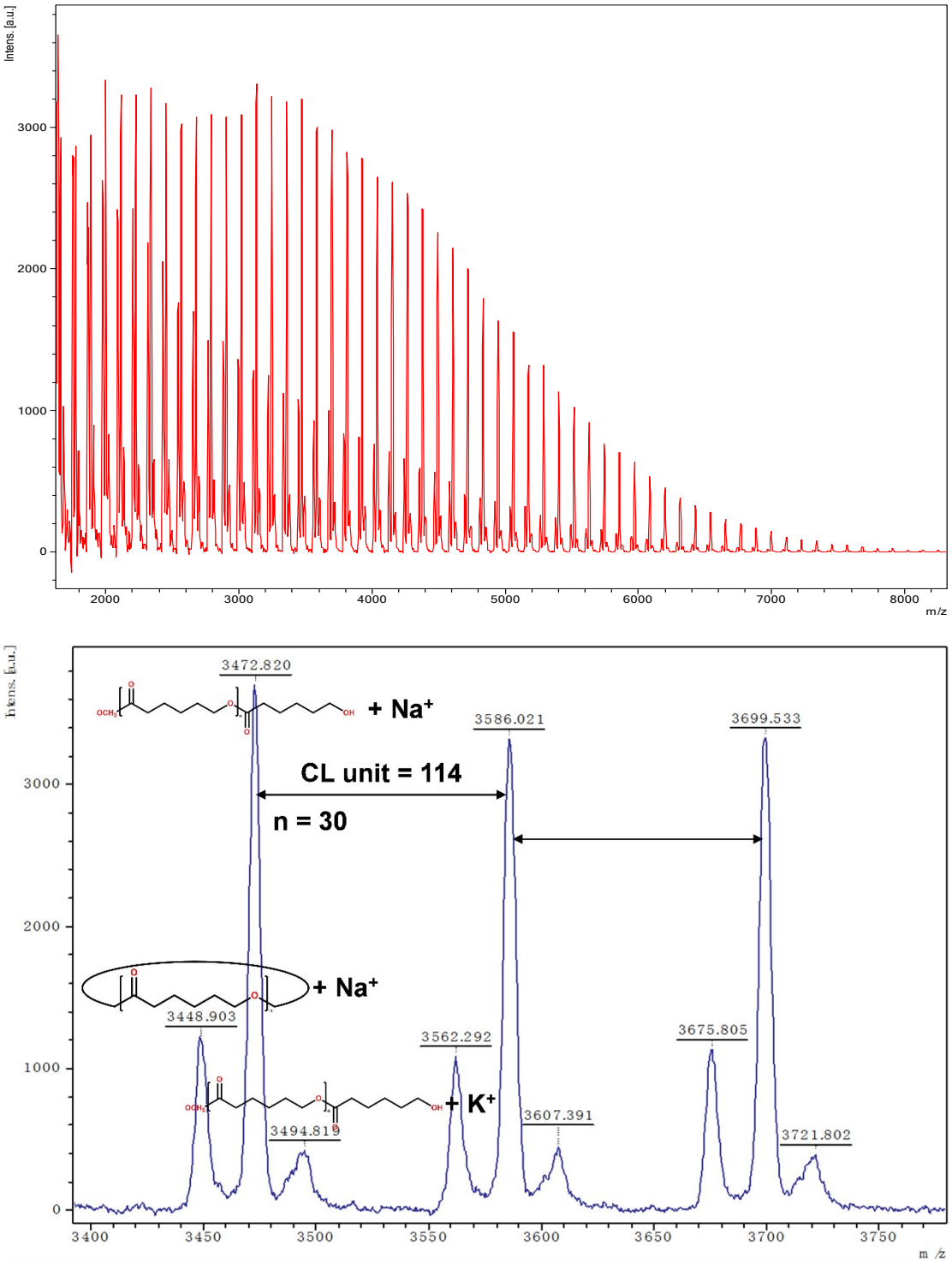

Figure S28. MALDI-TOF mass spectrum of PCL (Table 1, entry 7; Table S1; entry S14). The peak at *m/z* 3448.903 represents cyclic PCL with Na^+ (*m/z*: 114.1 x n + 23.0, n = 30), the peak at *m/z* 3472.820 represents the linear PCL $H_3CO(CL)_nH$ with Na^+ (*m/z*: 114.1 x n + 32.0 + 23.0, n = 30), the peak at *m/z* 3494.819 represents the linear PCL $H_3CO(CL)_nH$ with K^+ (*m/z*: 114.1 x n + 32.0 + 39.1, n = 30).

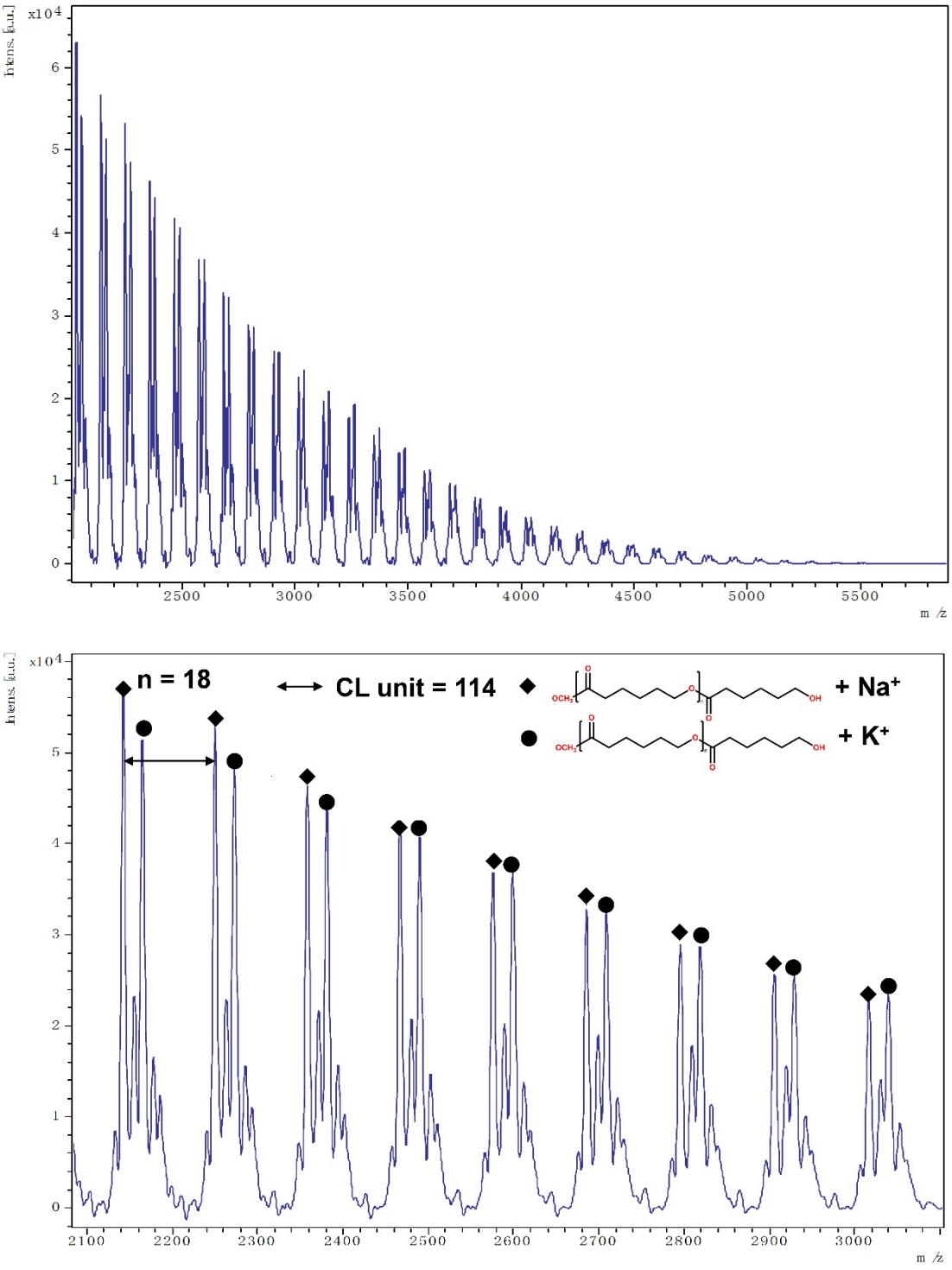

Figure S29. MALDI-TOF mass spectrum of PCL (Table S1; entry S16). The peak at *m/z* 2467.154 represents the linear PCL $H_3CO(CL)_nH$ with K^+ (*m/z*: 114.1 x n + 32.0 + 39.1, n = 21), the peak at *m/z* 2795.886 represents the linear PCL $H_3CO(CL)_nH$ with Na^+ (*m/z*: 114.1 x n + 32.0 + 23.0, n = 24).

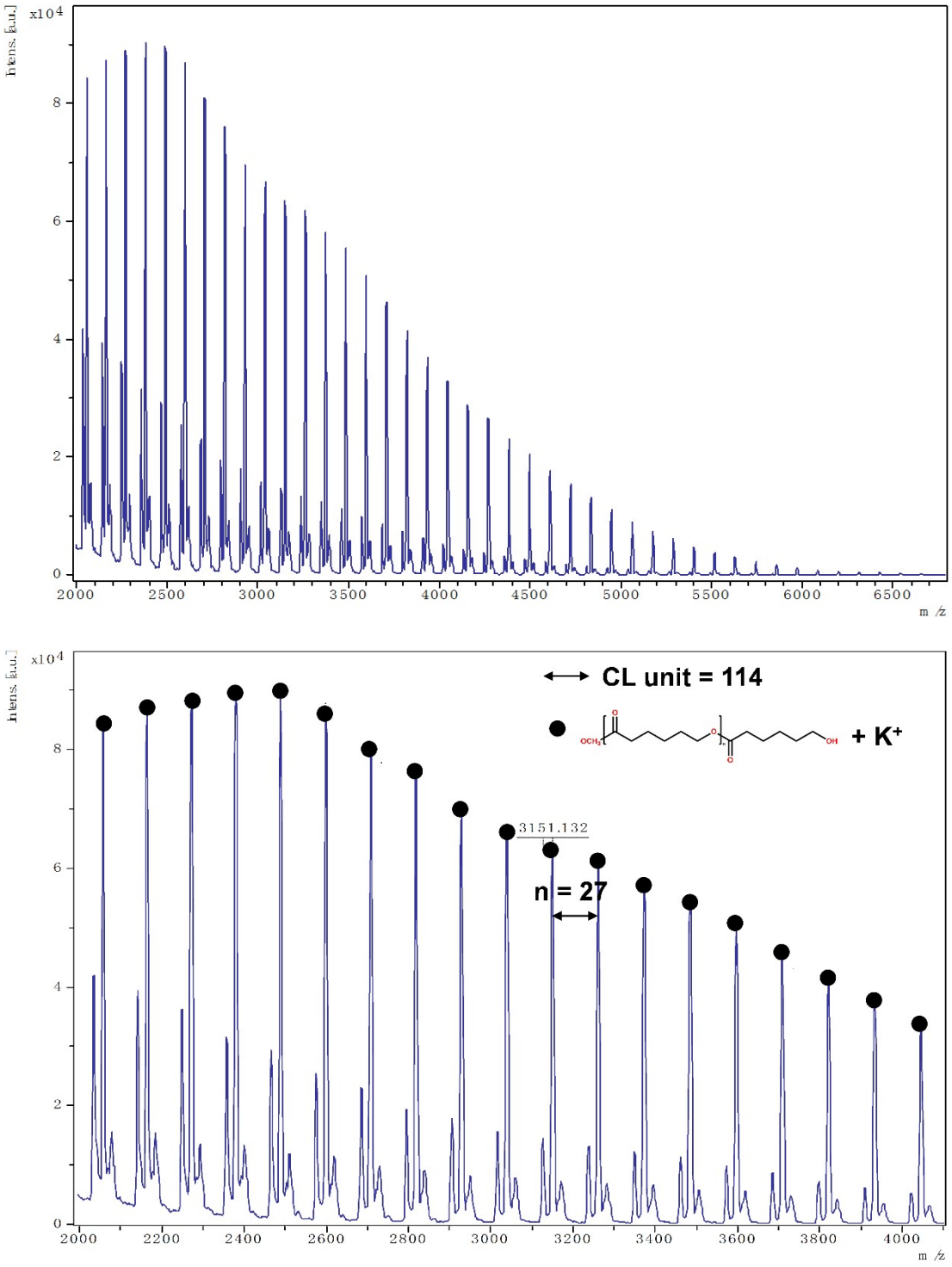

Figure S30. MALDI-TOF mass spectrum of PCL (Table S1, entry S18). The peak at *m/z* 3151.132 represents the linear PCL $H_3CO(CL)_nH$ with K^+ (*m/z*: 114.1 x n + 32.0 + 39.1, n = 27).

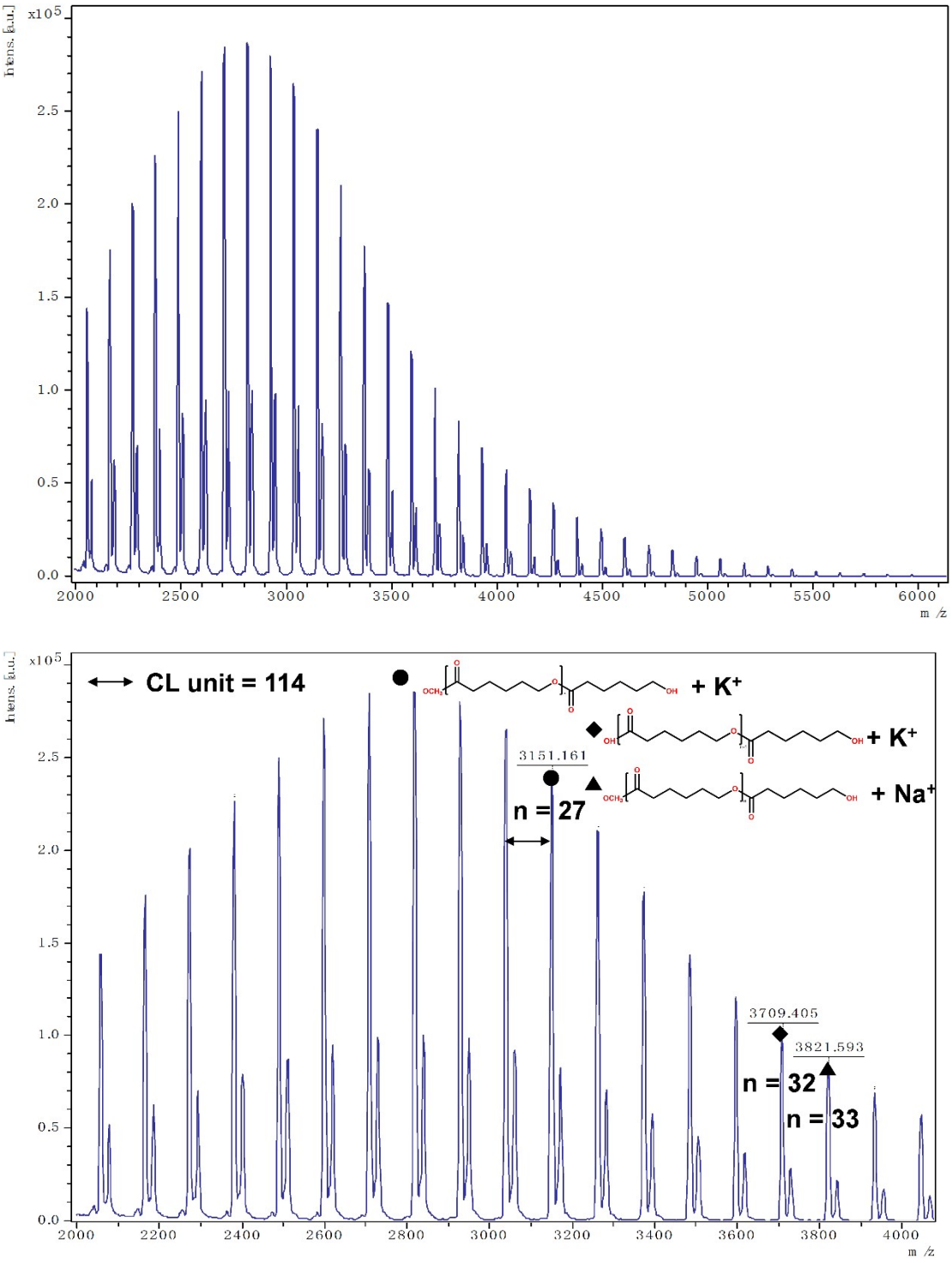

Figure S31. MALDI-TOF mass spectrum of PCL (Table 1, entry 10; Table S1, entry S20). The peak at *m/z* 3151.161 represents the linear PCL $H_3CO(CL)_nH$ with K^+ (*m/z*: 114.1 x n + 32.0 + 39.1, n = 27), the peak at *m/z* 3709.405 represents the linear PCL $HO(CL)_nH$ with K^+ (*m/z*: 114.1 x n + 18.0 + 39.1, n = 32), the peak at *m/z* 3821.593 represents the linear PCL $H_3CO(CL)_nH$ with Na^+ (*m/z*: 114.1 x n + 32.0 + 23.0, n = 33).

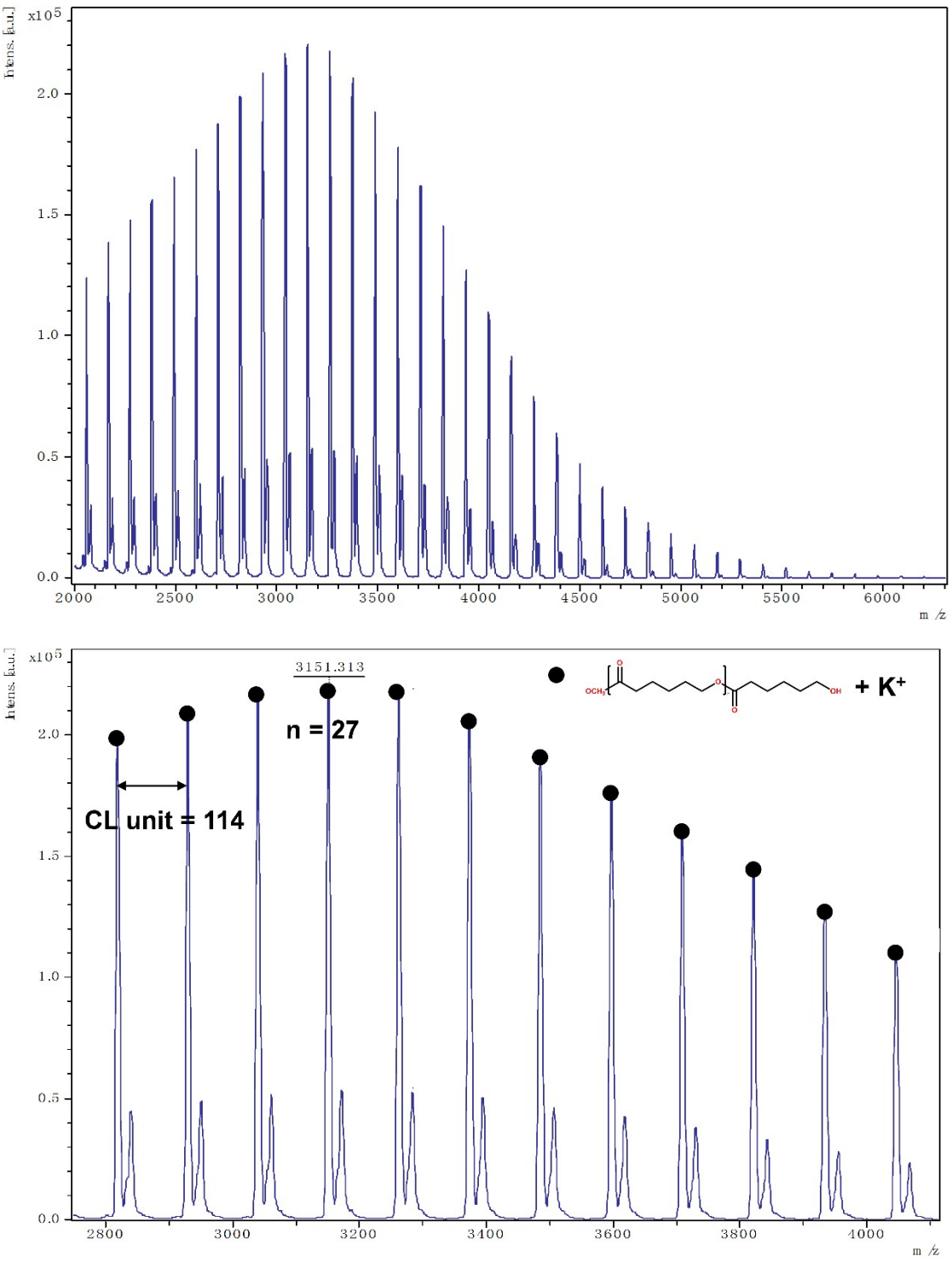

Figure S32. MALDI-TOF mass spectrum of PCL (Table 1, entry 11; Table S1, entry S22). The peak at *m/z* 3151.313 represents the linear PCL $H_3CO(CL)_nH$ with K^+ (*m/z*: 114.1 x n + 32.0 + 39.1, n = 27).

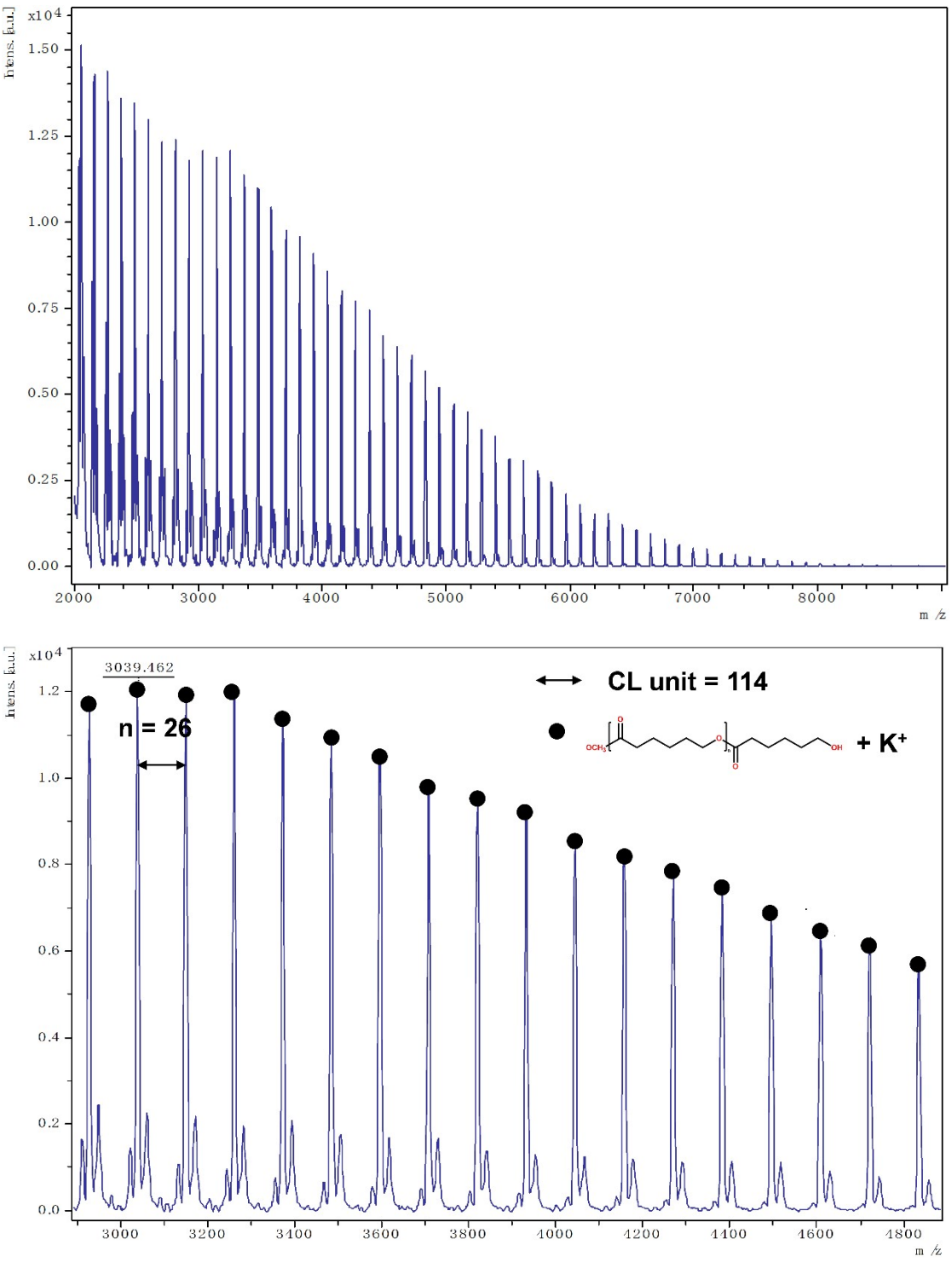

Figure S33. MALDI-TOF mass spectrum of PCL (Table 1, entry 12; Table S1, entry S24). The peak at *m/z* 3039.462 represents the linear PCL $H_3CO(CL)_nH$ with K^+ (*m/z*: 114.1 x n + 32.0 + 39.1, n = 26).

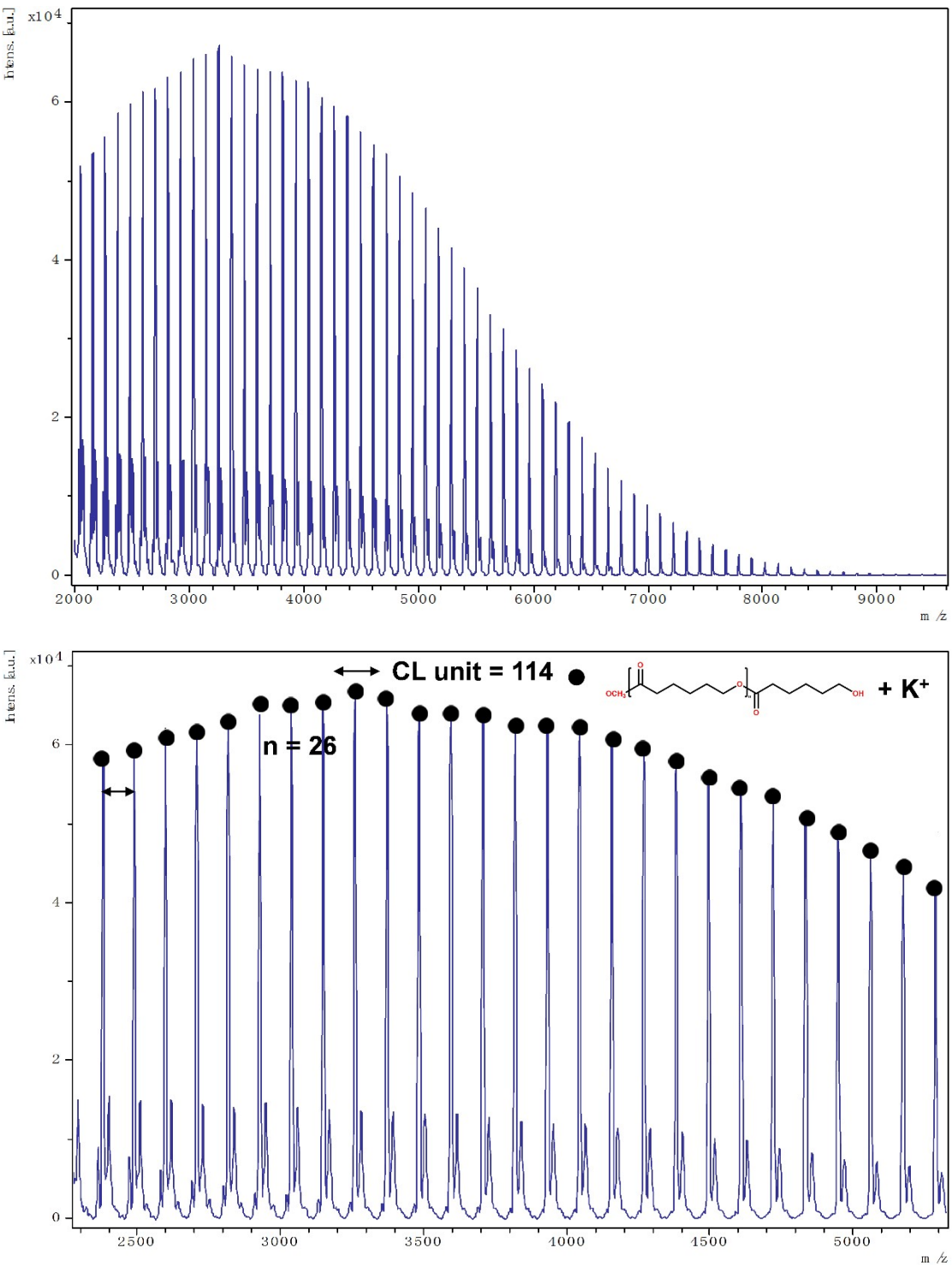

Figure S34. MALDI-TOF mass spectrum of PCL (Table S1, entry S26). The peak at *m/z* 3039.169 represents the linear PCL $H_3CO(CL)_nH$ with K^+ (*m/z*: 114.1 x n + 32.0 + 39.1, n = 26).

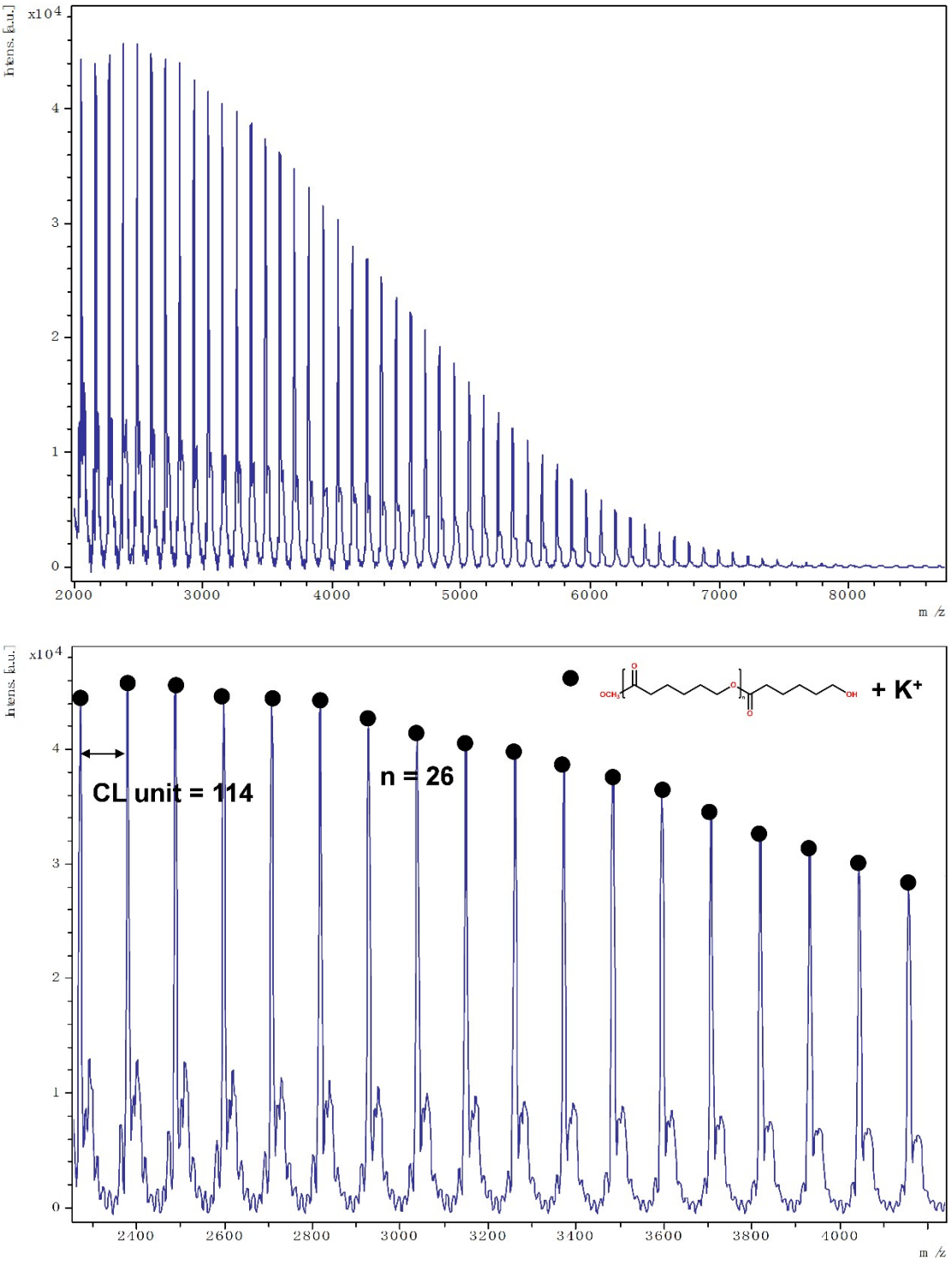

Figure S35. MALDI-TOF mass spectrum of PCL (Table S1; entry S28). The peak at *m/z* 3039.134 represents the linear PCL $H_3CO(CL)_nH$ with K^+ (*m/z*: 114.1 x n + 32.0 + 39.1, n = 26).

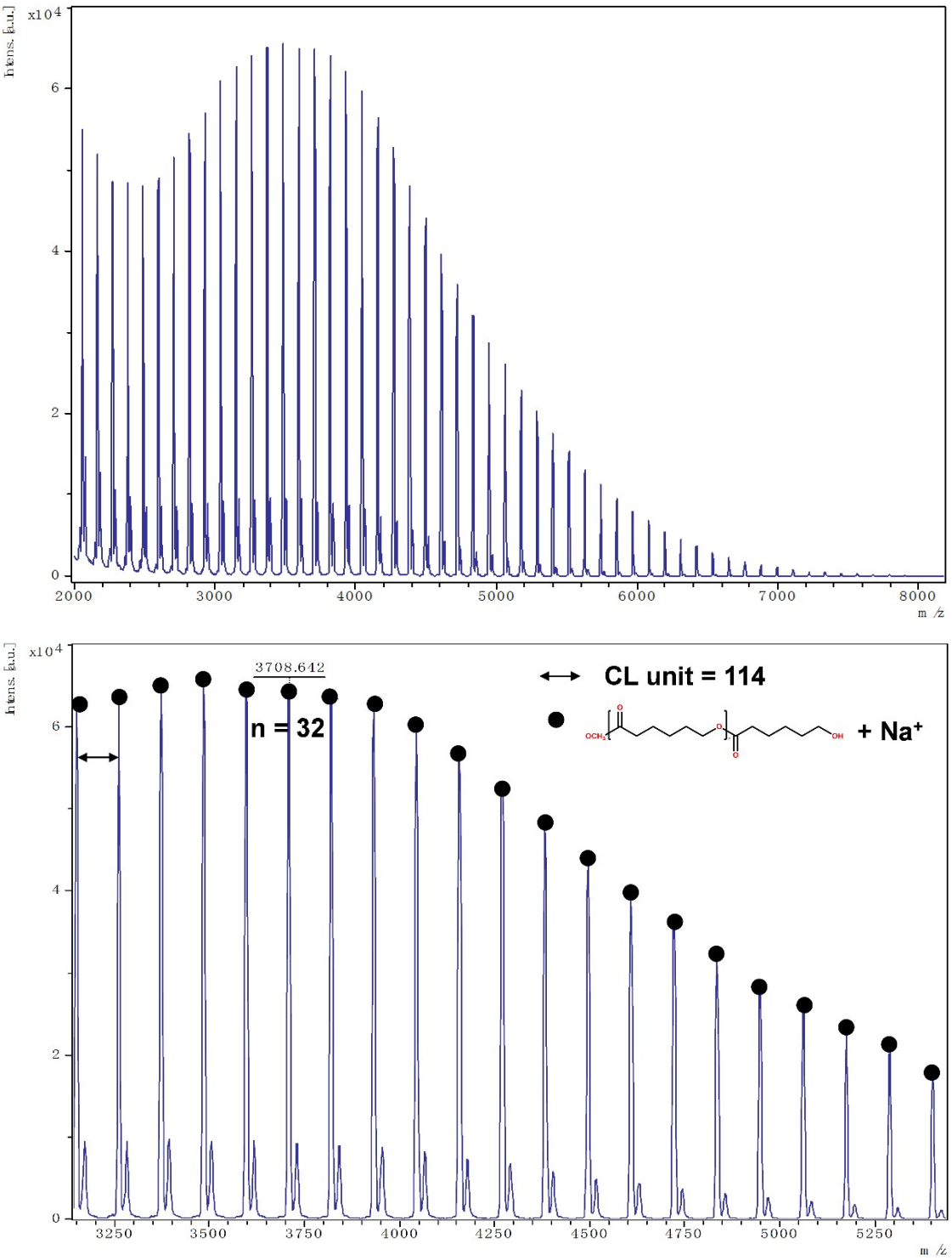

Figure S36. MALDI-TOF mass spectrum of PCL (Table S1, entry S30). The peak at *m/z* 3708.642 represents the linear PCL $H_3CO(CL)_nH$ with Na^+ (*m/z*: 114.1 x n + 32.0 + 23.0, n = 32).

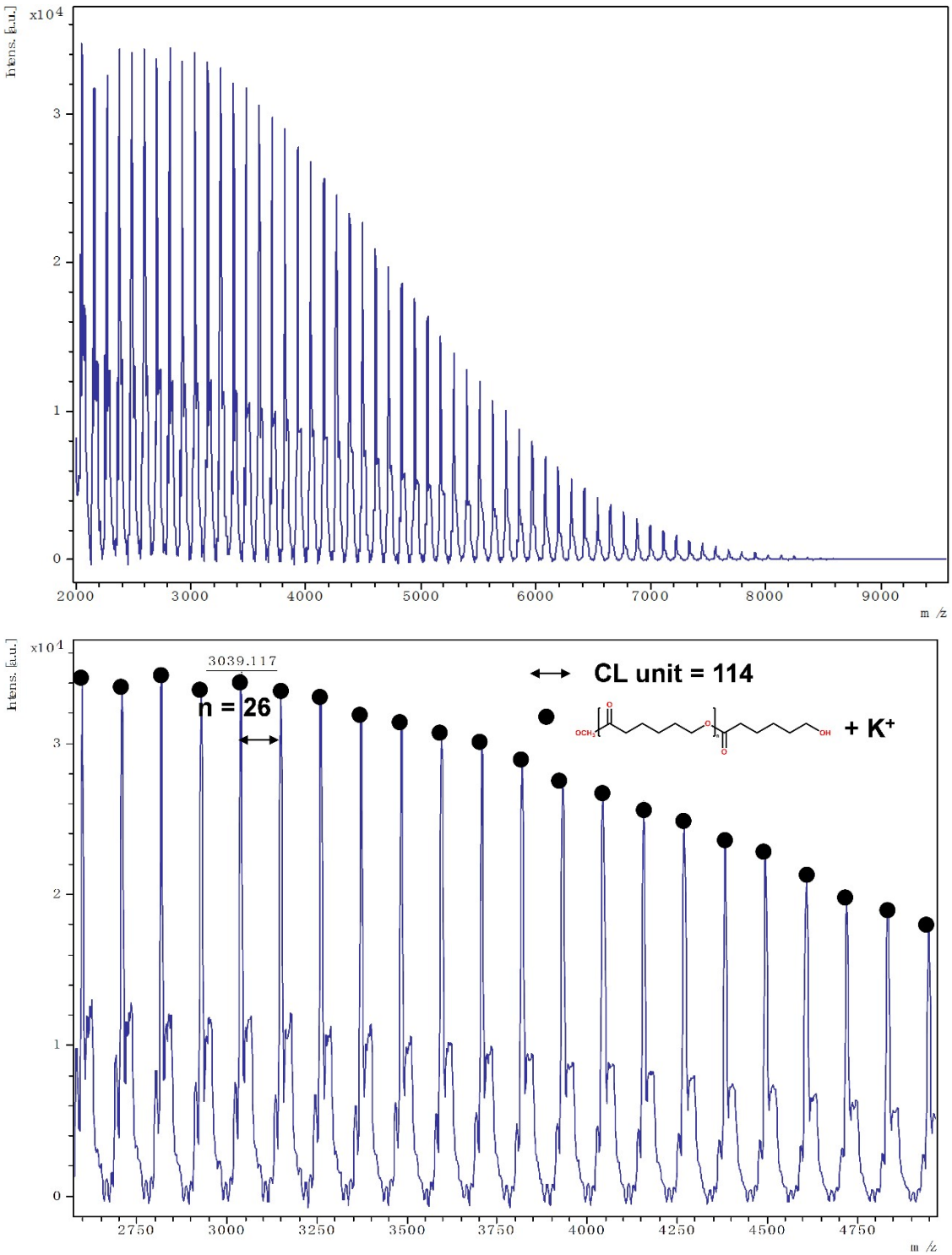

Figure S37. MALDI-TOF mass spectrum of PCL (Table 1, entry 16; Table S1, entry S32). The peak at *m/z* 3039.117 represents the linear PCL $H_3CO(CL)_nH$ with K^+ (*m/z*: 114.1 x n + 32.0 + 39.1, n = 26).

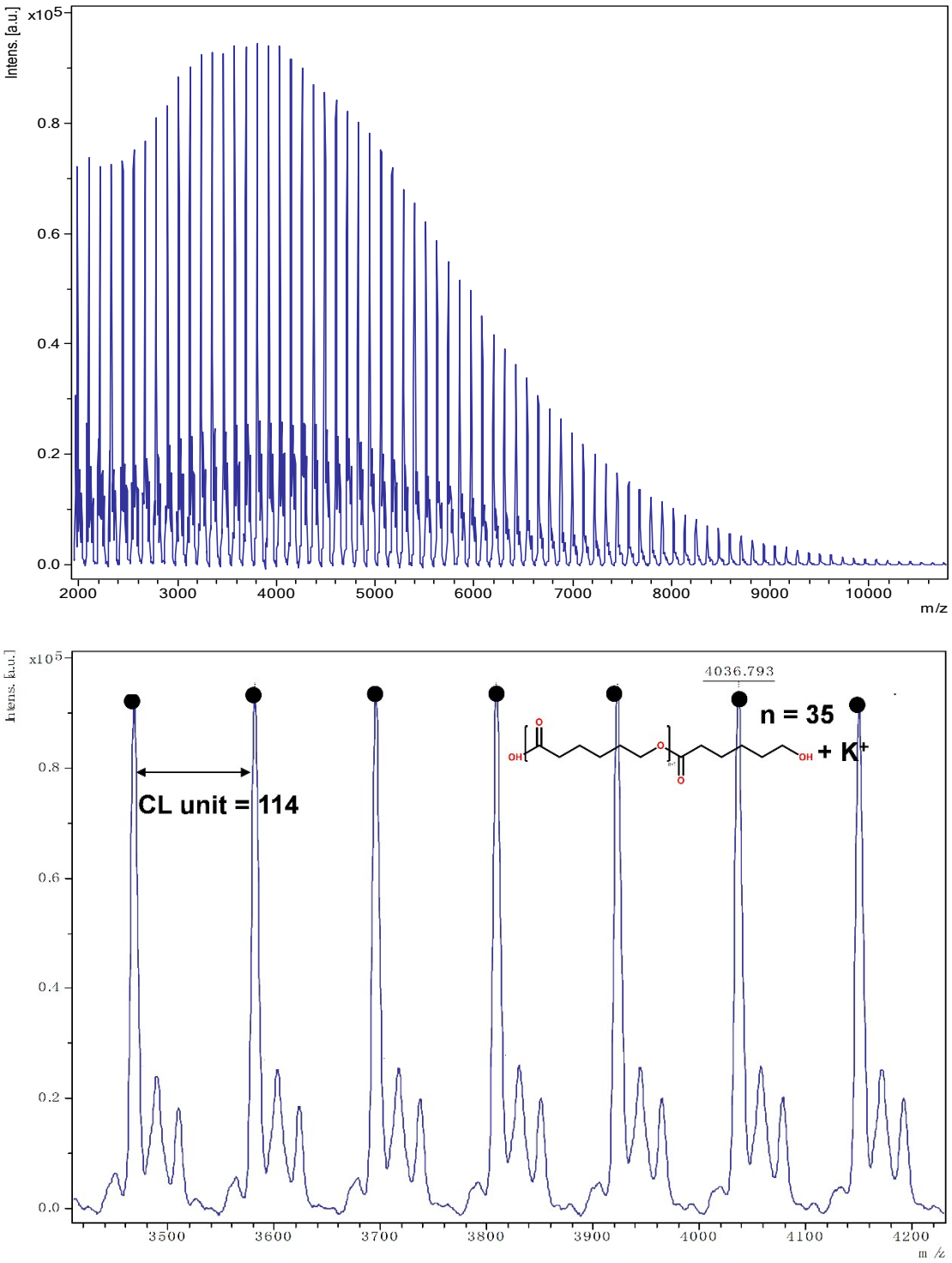

Figure S38. MALDI-TOF mass spectrum of PCL (Table 1, entry 34; Table S1, entry S34). The peak at *m/z* 4036.793 represents the linear PCL $HO(CL)_nH$ with K^+ (*m/z*: 114.1 x n + 18.0 + 39.1, n = 35).

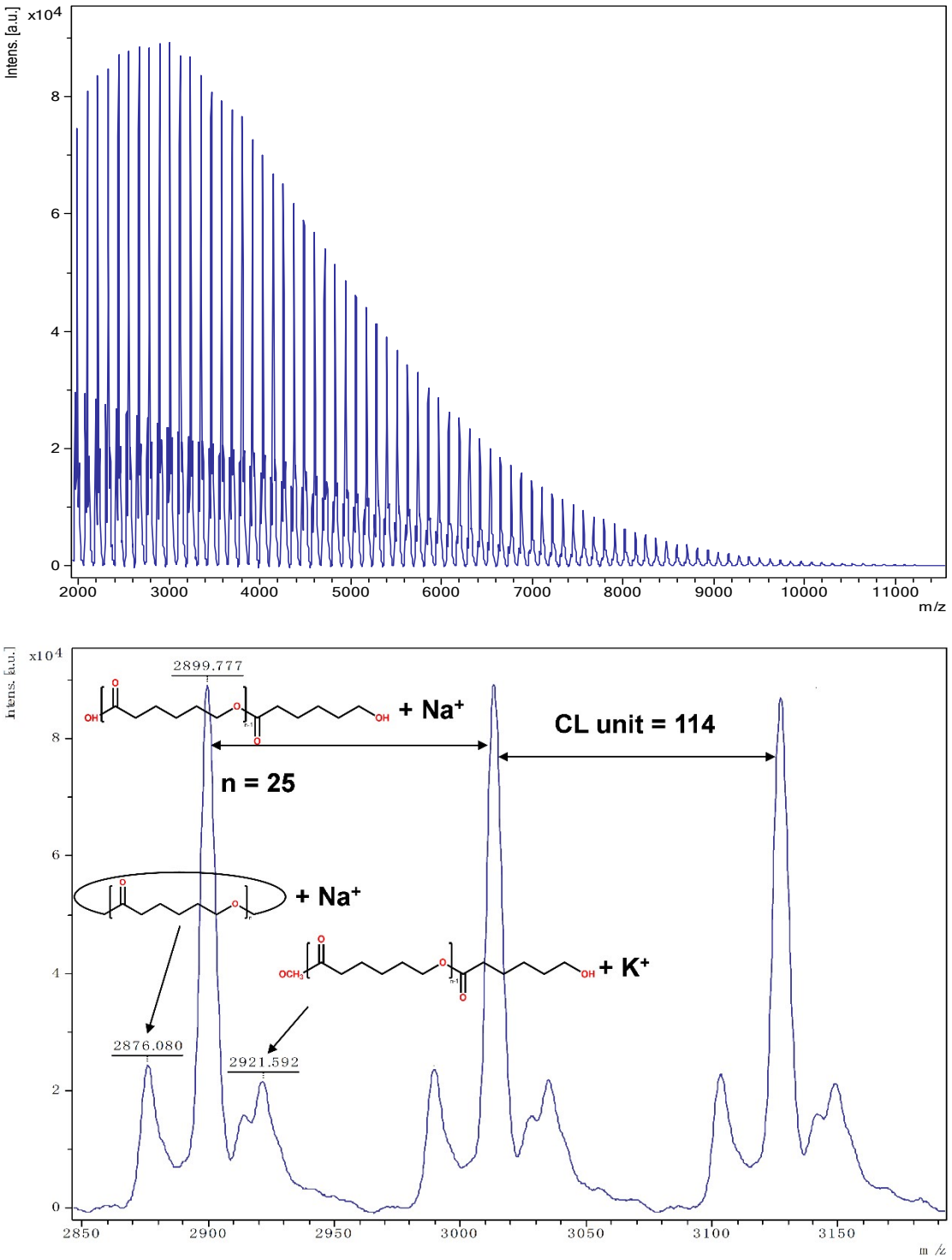

Figure S39. MALDI-TOF mass spectrum of PCL (Table 1, entry 36; Table S1, entry S36). The peak at *m/z* 2876.080 represents cyclic PCL with Na^+ (*m/z*: 114.1 x n + 23.0, n = 25), the peak at *m/z* 2899.777 represents the linear PCL $HO(CL)_nH$ with Na^+ (*m/z*: 114.1 x n + 18.0 + 23.0, n = 25), the peak at *m/z* 2921.592 represents the linear PCL $H_3CO(CL)_nH$ with K^+ (*m/z*: 114.1 x n + 32.0 + 39.1, n = 25).

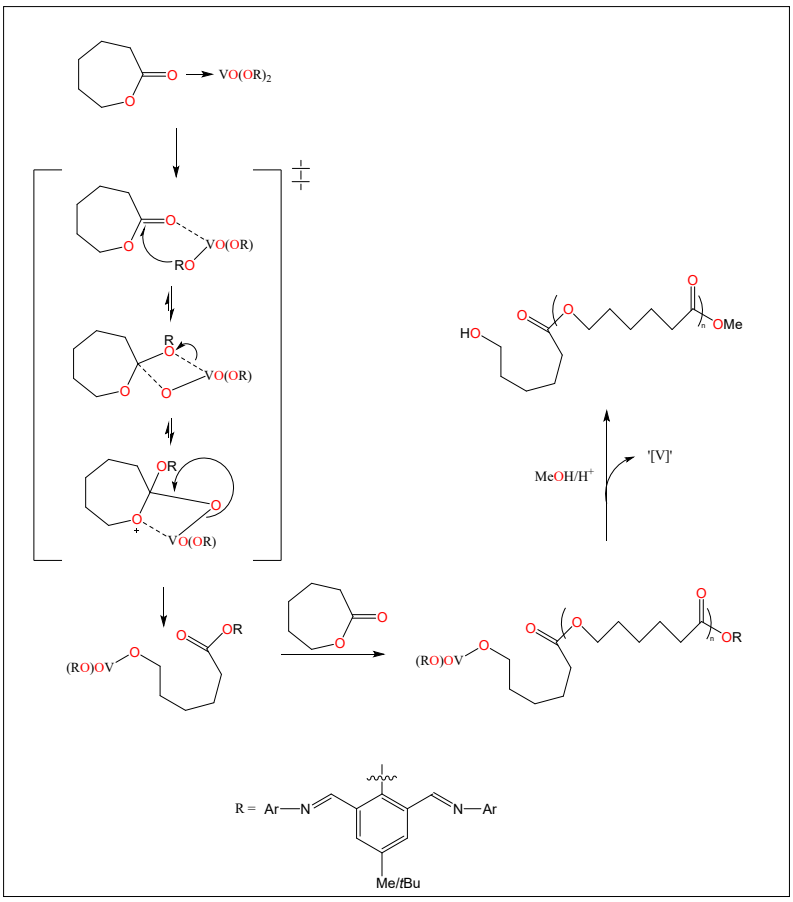

Figure 40. Proposed coordinative insertion mechanism.

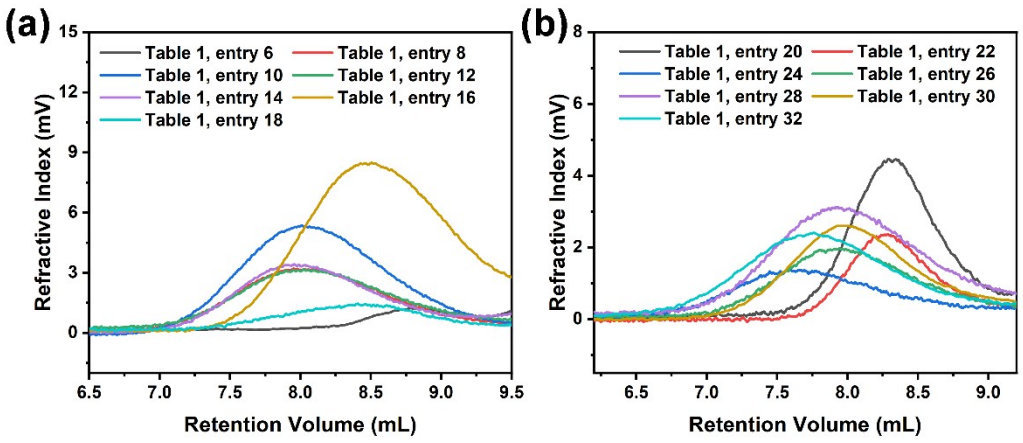

Figure S41. GPC trace of PCL from table 1, entries 6, 8, 10, 12, 14, 16, 18, 20, 22, 24, 26, 28, 30, 32.

The comparison with other published vanadium complexes in our group and one complex from Białek's group is shown in Table S3. [S4-S6] Polycaprolactones with lower molecular weight were obtained via the ROP initiated by vanadium complexes derived from *O*,*N*,*O*-tridentate 6-bis(o-

hydroxyalkyl/aryl)pyridines. However, under air, in the absence of benzyl alcohol, at 130 ℃ in

Catalyst	Time	Temp. (℃)	[CL]:[V][a]:[BnOH]	Conv. (%)	M_n (Da)	$Đ$	Reference
6[b]	24 h	130	500:1:0	98	9760	1.95	This work
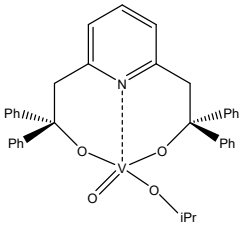	24 h	130	500:1:0	>99	6760	2.00	S4[b]
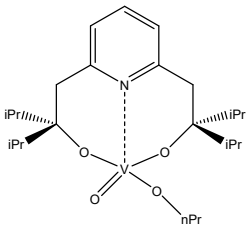	24 h	130	500:1:0	92	2510	1.35	S4[b]
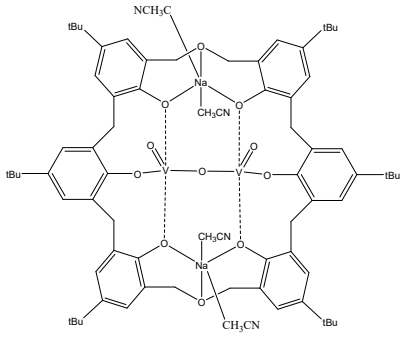	24 h	130	500:1:1	99	11610	1.41	S5[b]

toluene, the molecular weight of the resulting polymer was higher than that initiated by **6**. For the vanadium complex derived from oxacalix[6]arenes, the polymers obtained under conditions with the presence of benzyl alcohol exhibited a higher molecular weight compared with those reported in this paper. In contrast, the polymer resulting from the absence of benzyl alcohol showed a slightly lower molecular weight than the one initiated by **6**. Interestingly, another vanadium complex with an *O*,*N*,*O*-type ligand, namely [LV] (where LH_2 = 4,6-*t*Bu_2-2-(2-CH_2(OH)-C_6H_4N=CH)C_6H_3OH reported by Białek's group, afforded PCL with a molecular weight of 7400 Da in a shorter time (5 h) and at a lower temperature (120 ℃), but the conversion is only 42%. [S6]

Table S6. Comparison with other vanadium complexes.

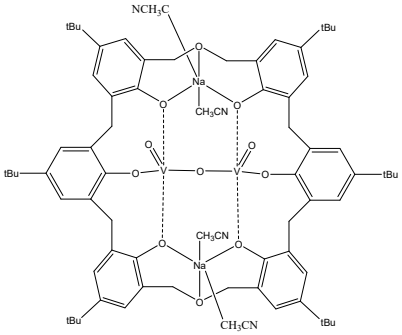	24 h	130	500:1:0	>99	8210	1.41	S5[b]
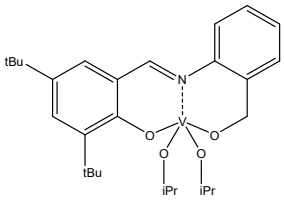	5 h	120	500:1:0	42	7400	1.60	S6[b]
6[c]	24 h	130	500:1:0	98	3440	1.86	This work
10[c]	24 h	130	500:1:0	99	10400	2.33	This work
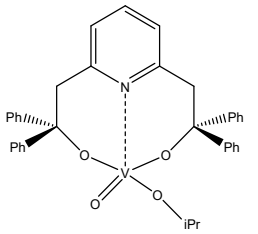	24 h	130	500:1:0	>99	7610	1.67	S4[c]
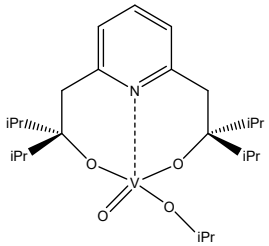	24 h	130	500:1:0	>99	4410	1.59	S4[c]
9[d]	24 h	130	500:1:0	86	10800	1.92	This work
10[d]	24 h	130	500:1:0	79	11650	2.24	This work
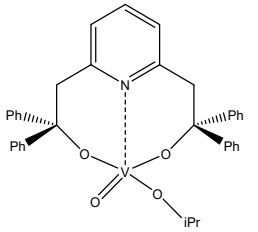	24 h	130	500:1:0	81	5280	2.14	S4[d]
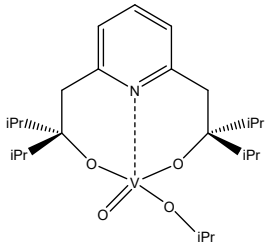	24 h	130	500:1:0	>99	5960	1.17	S4[d]
9[e]	24 h	130	500:1:0	77	9150	2.33	This work

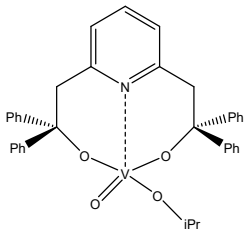	24 h	130	500:1:0	85	3090	2.06	S4[e]
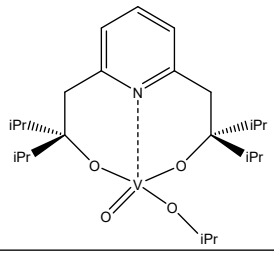	24 h	130	500:1:0	>99	3460	1.09	S4[e]

[a] Ratio of monomer to vanadium. [b] Conducted in toluene under nitrogen or argon. [c] Conducted in toluene under air. [d] Conducted as a melt under nitrogen. [e] Conducted as a melt under air.

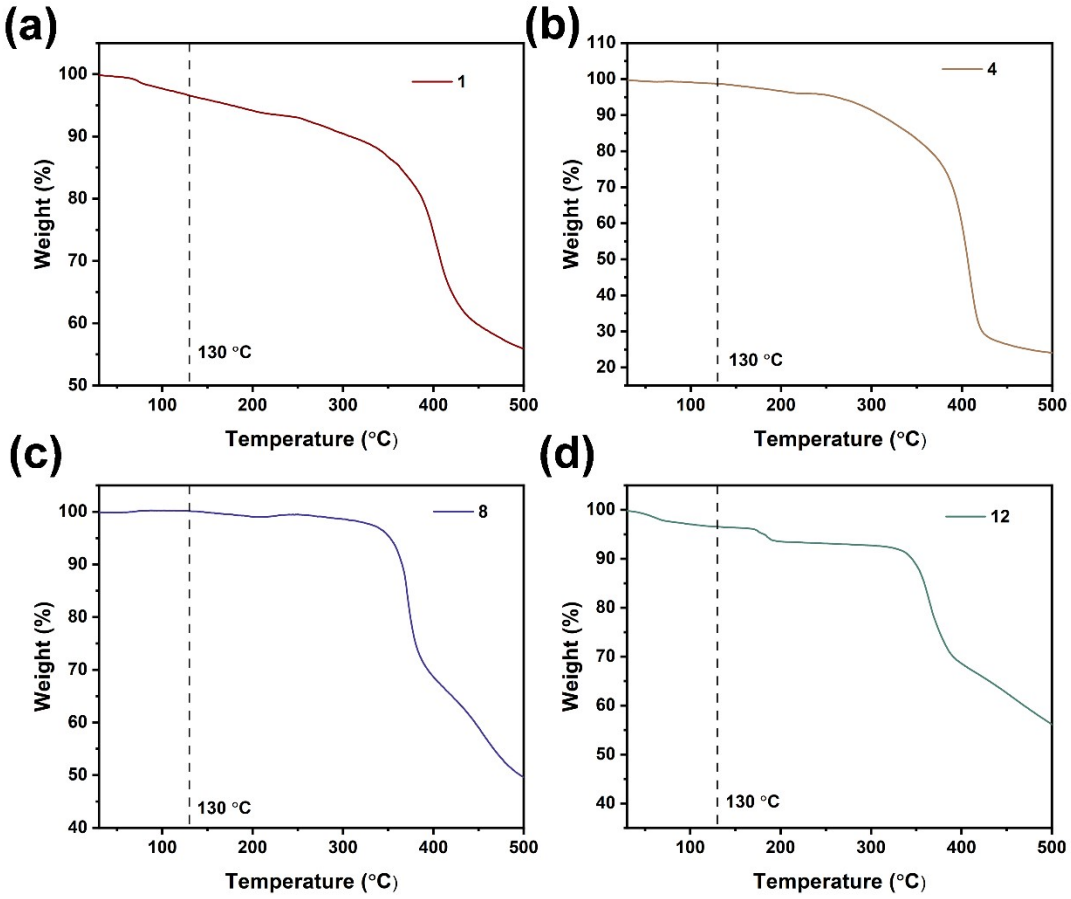

Figure S42. TGA of complexes **1**, **4**, **8** and **12.**

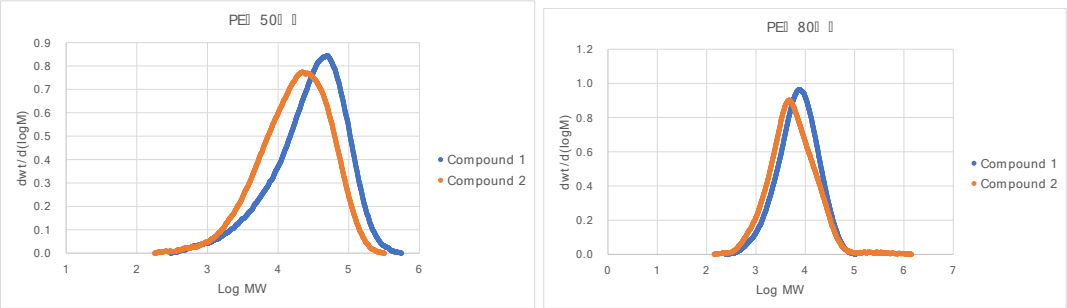

Figure S43. GPC curves of polyethylene formed by **1** and **2** using DEAC as co-catalyst. Entry designations refer to Table 3.

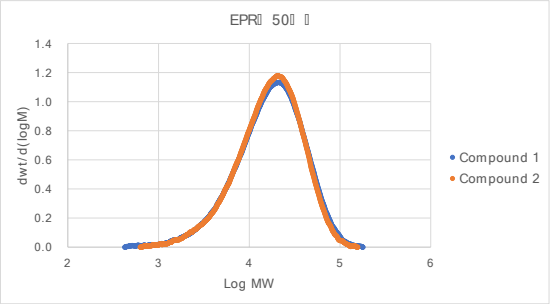

Figure S44. GPC curves of ethylene/propylene copolymer formed by **1** and **2** using DEAC as co-catalyst. Entry designations refer to Table 4.

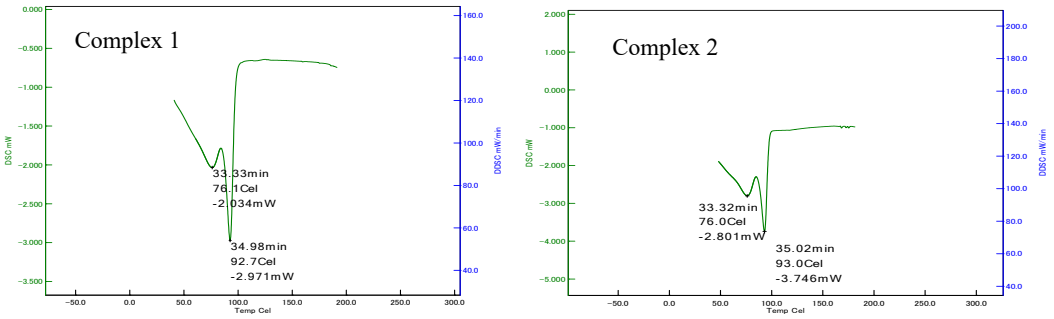

Figure S45. DSC thermograms of ethylene/propylene copolymer formed by **1** and **2** using DEAC as co-catalyst. Entry designations refer to Table 4.

References

[S1] L. Han, J. Du, H. Yang, H. Wang, X. Leng, A. Galstyan, S. Zarić and W. -H. Sun. *Inorg. Chem. Comm.*, 2003, **6**, 5-9.

[S2] L. Wang, W. -H. Sun, L. Han, Z. Li, Y. Hu, C. He and C. Yan. *J. Organomet. Chem.*, 2002,

650, 59-64.

[S3] M. Save, M. Schappacher and A. Soum. *Macromol. Chem. Phys*., 2002, **203**, 2591-2603.

[S4] M. R. J. Elsegood, W. Clegg and C. Redshaw, *Catalysts*, 2023, **13**, 988.

[S5] T. Xing, T. J. Prior, M. R. Elsegood, N. V. Semikolenova, I. E. Soshnikov, K. Bryliakov, K. Chen and C. Redshaw, *Catal. Sci. Technol.*, 2021, **11**, 624–636.

[S6] M. Białek, J. Fryga, G. Spaleniak and B. Dziuk, *J. Polym. Res.*, 2021, **28**, 79.